

Reexamining charmless $B \rightarrow PV$ decays in QCD factorization approach

Xinqiang Li^{1,2,3} and Yadong Yang¹ *

¹Department of Physics, Henan Normal University, Xinxiang, Henan 453007, P. R. China

²Institute of Theoretical Physics, Chinese Academy of Sciences, Beijing, 100080, P. R. China

³Graduate School of the Chinese Academy of Sciences, Beijing, 100039, P. R. China

September 27, 2018

Abstract

Using the QCD factorization approach, we reexamine the two-body hadronic charmless B -meson decays to final states involving a pseudoscalar (P) and a vector (V) meson, with inclusion of the penguin contractions of spectator-scattering amplitudes induced by the $b \rightarrow Dg^*g^*$ (where $D = d$ or s , and g^* denotes an off-shell gluon) transitions, which are of order α_s^2 . Their impacts on the CP -averaged branching ratios and CP -violating asymmetries are examined. We find that these higher order penguin contraction contributions have significant impacts on some specific decay modes. Since $B \rightarrow \pi K^*$, $K\rho$ decays involve the same electro-weak physics as $B \rightarrow \pi K$ puzzles, we present a detailed analysis of these decays and find that the five R -ratios for $B \rightarrow \pi K^*$, $K\rho$ system are in agreement with experimental data except for $R(\pi K^*)$. Generally, these new contributions are found to be important for penguin-dominated $B \rightarrow PV$ decays.

PACS Numbers: 13.25Hw, 12.15Mm, 12.38Bx.

*Corresponding author. E-mail address: yangyd@henannu.edu.cn

1 Introduction

The study of hadronic charmless B -meson decays can provide not only an interesting avenue to understand the CP violation and the flavor mixing of quark sector in the Standard Model (SM), but also powerful means to probe different new physics scenarios beyond the SM. With the operation of B -factory experiments, huge amount of experimental data on hadronic B -meson decays has been analyzed with appreciative precision. To account for the experimental data, theorists are urged to gain deep insight into the mechanism of rare hadronic B -meson decays, and to reduce theoretical uncertainties in determining the flavor parameters of the SM from experimental measurements.

In the past years, much progress has been made in understanding the hadronic charmless B -meson decays: several novel methods, such as the “naive” factorization (NF) [1], the perturbative QCD method (PQCD) [2], the QCD factorization (QCDF) [3], and the soft collinear effective theory (SCET) [4], have been proposed; in addition, some model-independent methods based on (approximate) flavor symmetries have also been used to analyze the rare hadronic B -meson decays [5, 6]. These methods usually have quite different understandings of the rare hadronic B -meson decays, and hence the corresponding predictions are also quite different. General comparison between these various methods can be found, for example, in Ref. [7]. Since we shall adopt the QCDF approach in this paper, we would only focus on this approach below.

The QCDF approach, put forward by Beneke *et al.* a few years ago, has been used widely to analyze the two-body hadronic B -meson decays [3, 8, 9, 10, 11, 12, 13]. The essence of the approach can be summarized as follows: since the b quark mass is much larger than the characteristic scale of hadronic interaction, Λ_{QCD} , to leading power in the heavy quark expansion, the hadronic matrix elements relevant to two-body hadronic B -meson decays can be factorized into perturbatively calculable hard scattering kernels and universal non-perturbative parts parameterized by the form factors and the meson light cone distribution amplitudes (LCDAs). This scheme has incorporated elements of the NF approach (as the leading contribution) and the hard-scattering approach (as the sub-leading corrections), and provides a powerful and systematical means to compute the radiative (sub-leading nonfactorizable) corrections to the NF approximation for the hadronic matrix elements. In particular, the strong phases, which

are very important for studying the CP violation in B -meson decays, are calculable from the first principle. Detailed proofs and arguments can be found in Ref. [3], and current status and recent developments of this approach have also been reviewed recently in [14].

In a recent work [13], we have studied the higher order penguin contractions of spectator-scattering amplitudes induced by the $b \rightarrow Dg^*g^*$ transitions (where $D = d$ or s , depends on the specific decay mode, and the off-shell gluons g^* are either emitted from the internal quark loops, external quark lines, or splitted off the virtual gluon of the penguin diagrams), and investigated their impacts on the CP -averaged branching ratios and CP -violating asymmetries of $B \rightarrow \pi\pi, \pi K$ decays. It has been found that these higher order penguin contraction contributions are not negligible in two-body hadronic B -meson decays, particularly in the penguin-dominated $B \rightarrow \pi K$ decays. Thus, combining the findings in the literature [15, 16, 17, 18], it would be worthy to take into account these higher order penguin contraction contributions to the exclusive hadronic B -meson decays. This encourages us to further investigate their impacts on the hadronic charmless $B \rightarrow PV$ (where P and V denote pseudoscalar and vector mesons, respectively) decays.

$B \rightarrow PV$ decays are closely related to their PP counterparts because of their similar flavor structures, however, these modes have apparent advantages in some cases. For example, due to the less penguin pollution, $B \rightarrow \pi\rho$ decay modes are more suitable than $B \rightarrow \pi\pi$ ones for extracting the weak angle α of the unitarity triangle of the Cabibbo-Kobayshi-Maskawa (CKM) matrix [20]. Studies on two-body hadronic $B \rightarrow PV$ decays are therefore very helpful to deepen our understandings of the rare hadronic B -meson decays. Earlier theoretical studies on $B \rightarrow PV$ decays based on various approaches can be found, for example, in Refs. [21, 22]. With the accumulation of new experimental data and the theoretical improvements, these $B \rightarrow PV$ decay modes have also been reanalyzed recently [6, 10, 11, 12]. In this paper, we will reexamine these hadronic charmless $B \rightarrow PV$ decays within the framework of QCDF approach and take into account the higher order penguin contractions of spectator-scattering amplitudes as mentioned above. Here we do not consider the decay modes with an η or η' meson in the final states, since in this case there are many additional unknown parameters pertaining to these two particles, such as their contents, mixing angles, and the anomaly $g-g-\eta^{(\prime)}$ coupling, which would hinder us from getting reliable theoretical predictions.

This paper is organized as follows. Sec. 2 is devoted to the theoretical framework. In this section, we first give the relevant formulas describing the decay amplitudes of hadronic $B \rightarrow PV$ decays at next-to-leading order in α_s , and then take into account contributions of the higher order penguin contractions of spectator-scattering amplitudes induced by the $b \rightarrow Dg^*g^*$ transitions. In Sec. 3, we give our numerical results for CP -averaged branching ratios and CP -violating asymmetries, and discuss the impacts of the higher order corrections on these quantities. Detailed analysis of the interesting decays $B \rightarrow \pi K^*$ and $B \rightarrow K\rho$, are also presented in this section. Finally, we conclude with a summary in Sec. 4. Some useful functions and the input parameters used in this paper are collected in Appendix A and B, respectively.

2 Theoretical framework for $B \rightarrow PV$ decays

2.1 The effective Hamiltonian for hadronic B -meson decays

Using the operator product expansion (OPE) and the renormalization group equation (RGE), the low energy effective Hamiltonian for hadronic charmless B -meson decays in the SM can be written as [23]

$$\mathcal{H}_{\text{eff}} = \frac{G_F}{\sqrt{2}} \sum_{p=u,c} \lambda_p^{(\prime)} \left(C_1 Q_1^p + C_2 Q_2^p + \sum_{i=3,\dots,10} C_i Q_i + C_{7\gamma} Q_{7\gamma} + C_{8g} Q_{8g} \right) + \text{h.c.}, \quad (1)$$

where $\lambda_p = V_{pb} V_{ps}^*$ (for $b \rightarrow s$ transition) and $\lambda_p' = V_{pb} V_{pd}^*$ (for $b \rightarrow d$ transition) are products of the CKM matrix elements, and the unitarity relation $-\lambda_t^{(\prime)} = \lambda_u^{(\prime)} + \lambda_c^{(\prime)}$ has been used. The effective operators, Q_i , governing a given decay process, can be expressed explicitly as follows.

(i) Current-current operators:

$$Q_1^p = (\bar{p}b)_{V-A} (\bar{D}p)_{V-A}, \quad Q_2^p = (\bar{p}_i b_j)_{V-A} (\bar{D}_j p_i)_{V-A}, \quad (2)$$

(ii) QCD-penguin operators:

$$\begin{aligned} Q_3 &= (\bar{D}b)_{V-A} \sum_q (\bar{q}q)_{V-A}, & Q_4 &= (\bar{D}_i b_j)_{V-A} \sum_q (\bar{q}_j q_i)_{V-A}, \\ Q_5 &= (\bar{D}b)_{V-A} \sum_q (\bar{q}q)_{V+A}, & Q_6 &= (\bar{D}_i b_j)_{V-A} \sum_q (\bar{q}_j q_i)_{V+A}, \end{aligned} \quad (3)$$

(iii) Electroweak penguin operators:

$$\begin{aligned}
Q_7 &= (\bar{D}b)_{V-A} \sum_q \frac{3}{2} e_q (\bar{q}q)_{V+A}, & Q_8 &= (\bar{D}_i b_j)_{V-A} \sum_q \frac{3}{2} e_q (\bar{q}_j q_i)_{V+A}, \\
Q_9 &= (\bar{D}b)_{V-A} \sum_q \frac{3}{2} e_q (\bar{q}q)_{V-A}, & Q_{10} &= (\bar{D}_i b_j)_{V-A} \sum_q \frac{3}{2} e_q (\bar{q}_j q_i)_{V-A},
\end{aligned} \tag{4}$$

(iv) Electro- and chromo-magnetic dipole operators:

$$Q_{7\gamma} = \frac{-e}{8\pi^2} m_b \bar{D} \sigma_{\mu\nu} (1 + \gamma_5) F^{\mu\nu} b, \quad Q_{8g} = \frac{-g_s}{8\pi^2} m_b \bar{D} \sigma_{\mu\nu} (1 + \gamma_5) G^{\mu\nu} b, \tag{5}$$

where $(\bar{q}_1 q_2)_{V\pm A} = \bar{q}_1 \gamma_\mu (1 \pm \gamma_5) q_2$, i, j are colour indices, e_q is the quark electric charge in units of $|e|$, and a summation over $q = u, d, s, c, b$ is implied. For $b \rightarrow d$ transition induced decay modes, $D = d$, while for $b \rightarrow s$ transition induced ones, $D = s$.

The Wilson coefficients $C_i(\mu)$ in Eq. (1) represent all the physics contributions higher than the scale $\mu \sim \mathcal{O}(m_b)$. Numerical results for these coefficients evaluated at different scales can be found in Ref. [23].

2.2 Decay amplitudes at next-to-leading order in α_s

With the low energy effective Hamiltonian given by Eq. (1), the decay amplitude for a general hadronic charmless $B \rightarrow PV$ decay can be written as

$$\langle PV | \mathcal{H}_{\text{eff}} | B \rangle = \frac{G_F}{\sqrt{2}} \sum_{p=u,c} \lambda_p^{(\prime)} C_i \langle PV | Q_i^p | B \rangle. \tag{6}$$

Then, the most essential theoretical problem in the calculation of the decay amplitude resides in the evaluation of the hadronic matrix elements of the local operators contained in the effective Hamiltonian, $\langle PV | Q_i^p | B \rangle$. With the QCDF approach, they could be simplified to a large extent. To leading power in Λ_{QCD}/m_b , but to all orders in perturbation theory, these hadronic matrix elements obey the following factorization formula [3]

$$\begin{aligned}
\langle PV | Q_i^p | B \rangle &= F_+^{B \rightarrow P} T_{V,i}^{\text{I}} * f_V \Phi_V + A_0^{B \rightarrow V} T_{P,i}^{\text{I}} * f_P \Phi_P \\
&\quad + T_i^{\text{II}} * f_B \Phi_B * f_P \Phi_P * f_V \Phi_V,
\end{aligned} \tag{7}$$

where Φ_M are the LCDAs of the meson M , the $*$ products indicate convolutions of the LCDAs and the hard-scattering kernels $T_i^{\text{I,II}}$. $F_+^{B \rightarrow P}$ and $A_0^{B \rightarrow V}$ denote the heavy-to-light $B \rightarrow P$ and

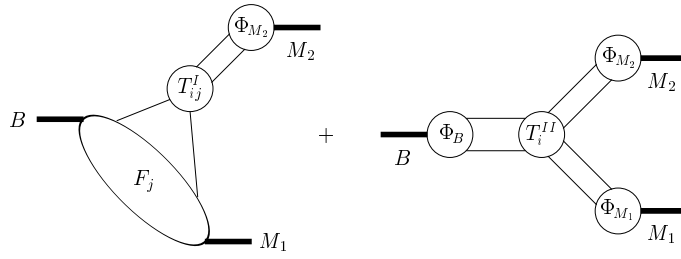


Figure 1: Graphical representation of the factorization formula. Only one of the two form-factor terms in Eq. (7) is shown for simplicity.

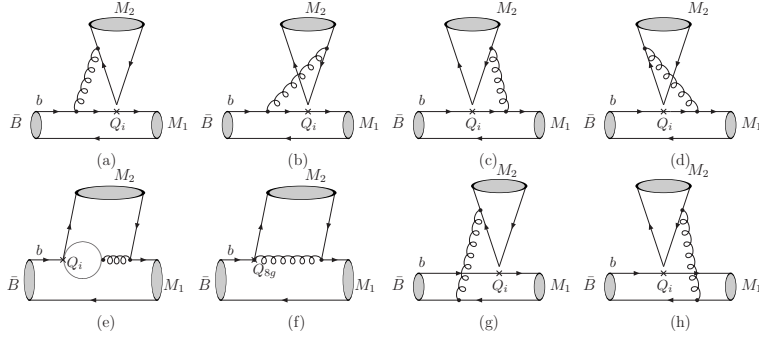


Figure 2: Order α_s corrections to the hard-scattering kernels $T_{M,i}^I$ (coming from the diagrams (a)-(f)) and T_i^{II} (coming from the last two diagrams).

$B \rightarrow V$ transition form factors, respectively. A graphical representation of this formula is shown in Fig. 1.

When the power suppressed $\mathcal{O}(\Lambda_{\text{QCD}}/m_b)$ terms are neglected, $T_i^{I,II}$ are dominated by hard gluon exchanges, and hence calculable order by order in perturbative QCD. The relevant Feynman diagrams contributing to these hard-scattering kernels at next-to-leading order in α_s are shown in Fig. 2. The kernel $T_{M,i}^I$ starts at tree level and, at next-to-leading order in α_s , contains the sub-leading “nonfactorizable” corrections coming from the vertex-correction diagrams Figs. 2(a-d) and the penguin diagrams Figs. 2(e-f). The kernel T_i^{II} contains the hard “nonfactorizable” interactions between the spectator quark and the emitted meson M_2 . Its lowest order contributions are of order α_s and can be depicted by the hard spectator-scattering diagrams Figs. 2(g-h). At leading order, $T_{M,i}^I = 1$, $T_i^{II} = 0$, the QCDF formula reproduce the NF results.

As stressed in Ref. [8], it should be borne in mind that the factorization formula, Eq. (7), does not imply that the hadronic B -meson decays are perturbative in nature. Dominant soft contributions to the decay amplitude do exist. However, all these nonperturbative effects either are power-suppressed by Λ_{QCD}/m_b or can be factorized into the transition form factors and the

meson LCDAs.

With the above discussions about the effective Hamiltonian for hadronic B -meson decays and the QCDF formula for the hadronic matrix element, the decay amplitude for a general hadronic charmless $B \rightarrow PV$ decay, in the heavy quark limit, can then be rewritten as

$$\mathcal{A}(B \rightarrow PV) = \frac{G_F}{\sqrt{2}} \sum_{p=u,c} \sum_{i=1}^{10} \lambda_p^{(\prime)} a_i^p \langle PV|Q_i|B \rangle_F, \quad (8)$$

where $\langle PV|Q_i|B \rangle_F$ is the factorized hadronic matrix element, which has the same definition as that in the NF approach. All the ‘‘nonfactorizable’’ effects are encoded in the coefficients a_i^p , which are process dependent and can be calculated perturbatively. Following Beneke *et al.* [12], the general form of the coefficients a_i^p ($i = 1, \dots, 10$) at next-to-leading order in α_s , with M_1 being the meson picking up the spectator quark and M_2 the emitted meson, can be written as

$$a_i^p(M_1 M_2) = (C_i + \frac{C_{i\pm 1}}{N_c}) N_i(M_2) + \frac{C_{i\pm 1}}{N_c} \frac{C_F \alpha_s}{4\pi} \left[V_i(M_2) + \frac{4\pi^2}{N_c} H_i(M_1 M_2) \right] + P_i^p(M_2), \quad (9)$$

where the upper (lower) signs apply when i is odd (even). The quantities $V_i(M_2)$ account for one-loop vertex corrections, $H_i(M_1 M_2)$ for hard-spectator interactions, and $P_i^p(M_2)$ for penguin contributions. Explicit expressions for these quantities can be found in Ref. [12].

It is noted that, in calculations of the decay amplitudes for hadronic charmless B -meson decays, the coefficients a_i^p ($i = 3, \dots, 10$) always appear in pairs. So, for the two-body hadronic charmless $B \rightarrow PV$ decays, one can define the following quantities α_i^p in terms of the coefficients a_i^p defined in Eq. (9) [12]

$$\begin{aligned} \alpha_1(M_1 M_2) &= a_1(M_1 M_2), \\ \alpha_2(M_1 M_2) &= a_2(M_1 M_2), \\ \alpha_3^p(M_1 M_2) &= \begin{cases} a_3^p(M_1 M_2) - a_5^p(M_1 M_2); & \text{if } M_1 M_2 = VP, \\ a_3^p(M_1 M_2) + a_5^p(M_1 M_2); & \text{if } M_1 M_2 = PV, \end{cases} \\ \alpha_4^p(M_1 M_2) &= \begin{cases} a_4^p(M_1 M_2) + r_\chi^{M_2} a_6^p(M_1 M_2); & \text{if } M_1 M_2 = PV, \\ a_4^p(M_1 M_2) - r_\chi^{M_2} a_6^p(M_1 M_2); & \text{if } M_1 M_2 = VP, \end{cases} \\ \alpha_{3,ew}^p(M_1 M_2) &= \begin{cases} a_9^p(M_1 M_2) - a_7^p(M_1 M_2); & \text{if } M_1 M_2 = VP, \\ a_9^p(M_1 M_2) + a_7^p(M_1 M_2); & \text{if } M_1 M_2 = PV, \end{cases} \\ \alpha_{4,ew}^p(M_1 M_2) &= \begin{cases} a_{10}^p(M_1 M_2) + r_\chi^{M_2} a_8^p(M_1 M_2); & \text{if } M_1 M_2 = PV, \\ a_{10}^p(M_1 M_2) - r_\chi^{M_2} a_8^p(M_1 M_2); & \text{if } M_1 M_2 = VP, \end{cases} \end{aligned} \quad (10)$$

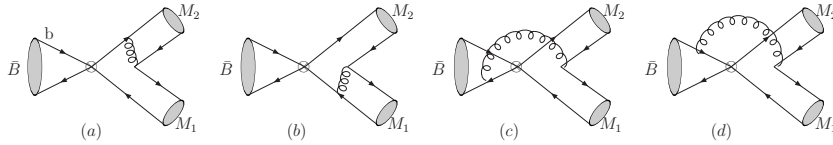


Figure 3: The weak annihilation diagrams of order α_s .

with the scale-dependent ratio $r_\chi^{M_2}$ defined as

$$r_\chi^P(\mu) = \frac{2m_P^2}{m_b(\mu)(m_{q_1} + m_{q_2})(\mu)}, \quad r_\chi^V(\mu) = \frac{2m_V}{m_b(\mu)} \frac{f_V^\perp(\mu)}{f_V}, \quad (11)$$

where all quark masses are running current masses defined in the $\overline{\text{MS}}$ scheme, and $f_V^\perp(\mu)$ is the scale-dependent transverse decay constant of vector meson. Although all these terms proportional to $r_\chi^{M_2}$ are formally power suppressed by Λ_{QCD}/m_b in the heavy-quark limit, they are not small numerically. In particular, the factor $r_\chi^P(\mu)$ is chirally enhanced and important for charmless B decays [8, 12].

According to the arguments in [3], the weak annihilation contributions to the decay amplitudes are power suppressed, and hence do not appear in the QCDF formula, Eq. (7). Nevertheless, these contributions may be numerically important for realistic B -meson decays. At order $\mathcal{O}(\alpha_s)$, the annihilation kernels arise from the four diagrams shown in Fig. 3. They result in a further contribution to the hard scattering kernel T_i^Π in the QCDF formula, Eq.(7). However, within the QCDF formalism, these annihilation topologies violate factorization because of the end-point divergence. In this work, following the treatment of Refs. [8, 24], we will introduce a cutoff to parameterize these contributions and express the weak annihilation decay amplitudes as

$$\mathcal{A}^{\text{ann}}(B \rightarrow PV) \propto \frac{G_F}{\sqrt{2}} \sum_{p=u,c} \sum_i \lambda_p^{(i)} f_B f_{M_1} f_{M_2} b_i(M_1 M_2), \quad (12)$$

where f_B and f_M are the decay constants of the initial B and the final-state mesons, respectively. The parameters $b_i(M_1 M_2)$ describe the annihilation contributions and their explicit expressions can be found in Refs. [8, 12].

The explicit expressions of the decay amplitudes for hadronic charmless $B \rightarrow PV$ decays, including the weak annihilation contributions, can be found, for example, in Refs. [11, 12]. It should be noted that, within the QCDF framework, all the “nonfactorizable” power suppressed contributions except for the hard spectator interactions and weak annihilation contributions are neglected. In addition, in the evaluation of the hard spectator and weak annihilation terms, the

running coupling constant and the Wilson coefficients should be evaluated at an intermediate scale $\mu_h \sim (\Lambda_{\text{QCD}} m_b)^{1/2}$ rather than the scale $\mu \sim m_b$. However, the evolution of $C_i(\mu)$ down to μ_h is highly nontrivial, since the RGE will change below the scale m_b . To deal with this problem, one may have to turn to SCET which is the appropriate effective theory for QCD below the m_b scale. However, in this paper, we restrict ourself to QCDF and adopt the treatments of evolution of the $C_i(\mu)$ as done in [8], i.e., we do not take into account the charm and bottom threshold and evolve the Wilson coefficients in a 5-flavored theory. With this approximation, in the evolution of the Wilson coefficients, all logs of the form $\log \mu/M_W$ have been summed, while logs of the form $\log \mu/m_b$ and $\log \mu/m_c$ are not. Since the latter two terms are never large with $\mu \geq m_b/2$, the approximation would work to the precision in this paper.¹ Specifically, we shall use $\mu_h = \sqrt{\Lambda_h \mu}$ with $\Lambda_h = 0.5$ GeV in our numerical calculations.

2.3 Penguin contractions of spectator-scattering amplitudes and their contributions to $B \rightarrow PV$ decays

At the quark level, the $b \rightarrow Dg^*g^*$ transitions can occur in many different manners as depicted by Figs. 4–6. For example, one of the two off-shell gluons can radiate from the external quark line, while the other one comes from the chromo-magnetic dipole operator Q_{8g} as Figs. 5(b) and 5(c) or from the internal quark loops of the penguin diagrams as Figs. 6(b) and 6(c). On the other hand, the two off-shell gluons can also radiate from the internal quark loops as Figs. 6(d) and 6(e) or split off the virtual gluon of the penguin diagrams as Figs. 5(a) and 6(a). Here we do not consider the Feynman diagrams of the category shown in Fig. 4, since their contributions can be absorbed into the definitions of heavy-to-light transition form factors as Figs. 4(a) and 4(b) and the meson LCDAs as Figs. 4(e), or are further suppressed by $\frac{1}{16\pi^2}$ as Figs. 4(c) and 4(d). It is easy to clarify this point by comparing the strength of Fig. 4(c) to that of Fig. 5(a).

As shown by Figs. 5 and 6, these Feynman diagrams should be the dominant sources contributing to the penguin contractions of spectator-scattering amplitudes of order α_s^2 , *since they are not two-loop QCD diagrams, and hence there are no additional $\frac{1}{16\pi^2}$ suppression factor in their contributions compared to the genuine two-loop ones of order α_s^2 .* Studying these contribu-

¹We thank M. Beneke for pointing out this point to us.

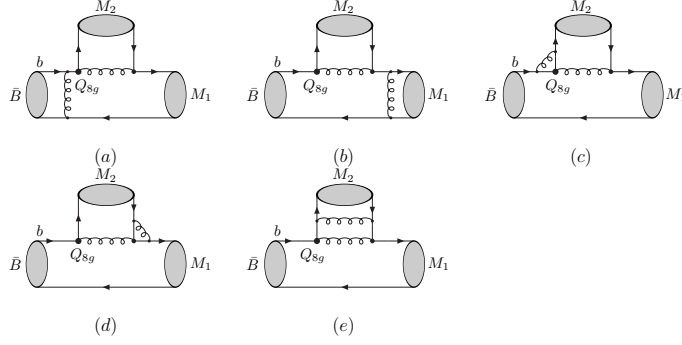


Figure 4: Representative Feynman diagrams induced by the $b \rightarrow Dg^*g^*$ transitions which are not needed to evaluate. Only the chromo-magnetic dipole operator Q_{8g} contributions are shown. With the operator Q_{8g} replaced by the other operators, the corresponding Feynman diagrams can also be obtained.

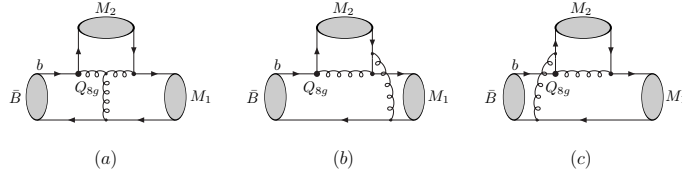


Figure 5: Chromo-magnetic dipole operator Q_{8g} contributions induced by the $b \rightarrow Dg^*g^*$ transitions.

tions could be very helpful for our understandings of the higher order perturbative corrections to the rare hadronic B -meson decays within the QCDF formalism.

We start with the calculations of the Feynman diagrams in Fig. 5. In this case, the b quark weak decay is induced by the chromo-magnetic dipole operator Q_{8g} , and the calculation is straightforward with the result given by

$$\begin{aligned}
\mathcal{A}_{Q_{8g}} &= i \frac{\alpha_s^2 f_B f_{M_1} f_{M_2}}{N_c^3} \lambda_t^{(\prime)} \int_0^1 d\xi \frac{\Phi_1^B(\xi)}{\xi} \\
&\times \int_0^1 dudv \left\{ \Phi_{M_2}(u) \Phi_{M_1}(v) \left[\frac{3(3-v)}{2(1-u)(1-v)v} + \frac{1}{6(1-u)(1-v)} \right] \right. \\
&+ r_\chi^{M_1} \Phi_{M_2}(u) \Phi_{m_1}(v) \left[\frac{3(3-u-v+uv)}{2(1-u)^2(1-v)v} + \frac{2-u}{6(1-u)u(1-v)} \right] \\
&+ r_\chi^{M_1} r_\chi^{M_2} \Phi_{m_2}(u) \Phi_{m_1}(v) \left[\frac{1}{6(1-u)(1-v)} + \frac{3(3-v)}{2(1-u)(1-v)v} \right] \\
&\left. + r_\chi^{M_2} \Phi_{m_2}(u) \Phi_{M_1}(v) \left[\frac{3(3-u-v-uv)}{2(1-u)(1-v)v} + \frac{1+u}{6(1-u)(1-v)} \right] \right\}, \quad (13)
\end{aligned}$$

when M_1 is a pseudoscalar and M_2 a vector meson. For the opposite case of a vector M_1 and a pseudoscalar M_2 , one needs only change the signs of the last two terms in the bracket of

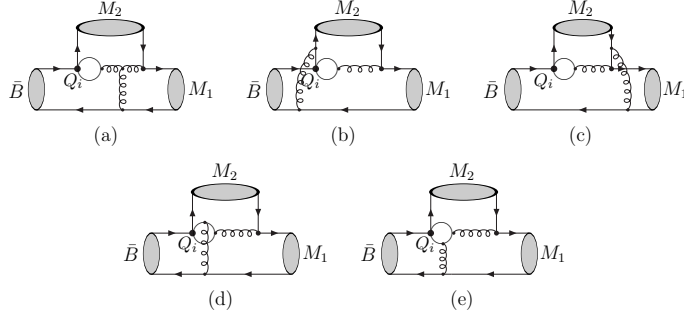


Figure 6: Penguin operator Q_i contributions induced by the $b \rightarrow Dg^*g^*$ transitions.

Eq. (13). Here $\lambda_t = V_{tb}V_{ts}^*$ and $\lambda'_t = V_{tb}V_{td}^*$ are products of the CKM matrix elements, Φ_M and Φ_m denote the leading-twist and twist-3 LCDAs of the meson M in the final states, respectively. In our calculation, we use the LCDAs in the asymptotic limit

$$\Phi_P(x) = \Phi_V(x) = 6x(1-x), \quad \Phi_p(x) = 1, \quad \Phi_v = 3(2x-1), \quad (14)$$

and have neglected the tree-particle LCDAs and deviations from the asymptotic limit.

In calculating the Feynman diagrams in Fig. 6, we adopt the method proposed by Greub and Liniger [17]. We first calculate the fermion loops in these individual Feynman diagrams, and then insert these building blocks into the entire Feynman diagrams to obtain the final results. In evaluating the internal quark loop diagrams, we shall adopt the naive dimensional regularization (NDR) scheme and the modified minimal subtraction ($\overline{\text{MS}}$) scheme. In addition, we shall adopt Feynman gauge for the gluon propagator throughout this paper. The gauge invariance will be guaranteed when the full set of Feynman diagrams are summed with the external quarks on-mass-shell [25]. However, we must be care of the gauge dependence in our calculation, since only a subset $\mathcal{O}(\alpha_s^2)$ Feynman diagrams are calculated. After careful checking, we find that each Feynman diagram in Fig.5. and 6 is gauge independent. The detail checking can be found in Appendix C. Analogous to the calculation of the penguin diagrams in Fig. 2(e), we should also take into account the two distinct penguin contractions of the four-quark operators in the weak interaction vertex .

As shown in Fig. 6, the first three Feynman diagrams have the same building block $I_\mu^a(k)$ (corresponding to contractions of the operators $Q_{1,3,9}$) or $\tilde{I}_\mu^a(k)$ (corresponding to contractions of the operators $Q_{4,6,8,10}$). These building blocks can be depicted by Fig. 7 and given by

$$I_\mu^a(k) = \frac{g_s}{4\pi^2} \Gamma\left(\frac{\epsilon}{2}\right) (2-\epsilon) (4\pi\mu^2)^{\frac{\epsilon}{2}} (k_\mu \not{k} - k^2 \gamma_\mu) (1-\gamma_5) T^a$$

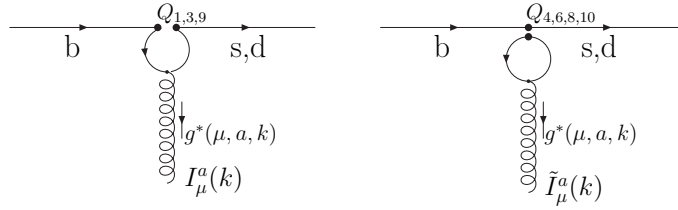


Figure 7: Building blocks $I_\mu^a(k)$ (corresponding to contractions of the operators $Q_{1,3,9}$) and $\tilde{I}_\mu^a(k)$ (corresponding to contractions of the operators $Q_{4,6,8,10}$) for Figs. 6(a)–6(c).

$$\times \int_0^1 dx \frac{x(1-x)}{\left[m_q^2 - x(1-x)k^2 - i\delta\right]^{\frac{\epsilon}{2}}}, \quad (15)$$

$$\begin{aligned} \tilde{I}_\mu^a(k) &= \frac{g_s}{2\pi^2} \Gamma\left(\frac{\epsilon}{2}\right) (4\pi\mu^2)^{\frac{\epsilon}{2}} (k_\mu \not{k} - k^2 \gamma_\mu) (1 - \gamma_5) T^a \\ &\times \int_0^1 dx \frac{x(1-x)}{\left[m_q^2 - x(1-x)k^2 - i\delta\right]^{\frac{\epsilon}{2}}}, \end{aligned} \quad (16)$$

where k is the momentum of the off-shell gluon, $T^a = \frac{\lambda^a}{2}$, with λ^a the Gell-Mann matrices, g_s is the strong coupling constant, and m_q the pole mass of the quark propagating in the fermion loops. We have used $d = 4 - \epsilon$. After performing the subtraction with the $\overline{\text{MS}}$ scheme, we get

$$I_\mu^a(k) = -\frac{g_s}{8\pi^2} \left[\frac{2}{3} - \frac{4}{3} \ln \frac{\mu}{m_b} - G(s_q, r) \right] (k_\mu \not{k} - k^2 \gamma_\mu) (1 - \gamma_5) T^a, \quad (17)$$

$$\tilde{I}_\mu^a(k) = -\frac{g_s}{8\pi^2} \left[-\frac{4}{3} \ln \frac{\mu}{m_b} - G(s_q, r) \right] (k_\mu \not{k} - k^2 \gamma_\mu) (1 - \gamma_5) T^a, \quad (18)$$

with the function $G(s_q, r)$ defined by

$$G(s_q, r) = -4 \int_0^1 dx x(1-x) \ln[s_q - x(1-x)r - i\delta], \quad (19)$$

where $s_q = m_q^2/m_b^2$, $r = k^2/m_b^2$, and the term $i\delta$ is the “ ϵ -prescription”. The free indices μ and a should be contracted with the gluon propagator when inserting these building blocks into the entire Feynman diagrams.

The sum of the fermion loops in the last two diagrams in Fig. 6 are denoted by the building block $J_{\mu\nu}^{ab}(k, p)$ (corresponding to contractions of the operators $Q_{1,3,9}$) or $\tilde{J}_{\mu\nu}^{ab}(k, p)$ (corresponding to contractions of the operators $Q_{4,6,8,10}$), which are depicted by Fig. 8. Using the decomposition advocated by [16, 17], these building blocks can be expressed as

$$J_{\mu\nu}^{ab}(k, p) = T_{\mu\nu}^+(k, p) \{T^a, T^b\} + T_{\mu\nu}^-(k, p) [T^a, T^b], \quad (20)$$

$$\tilde{J}_{\mu\nu}^{ab}(k, p) = \tilde{T}_{\mu\nu}^+(k, p) \{T^a, T^b\} + \tilde{T}_{\mu\nu}^-(k, p) [T^a, T^b], \quad (21)$$

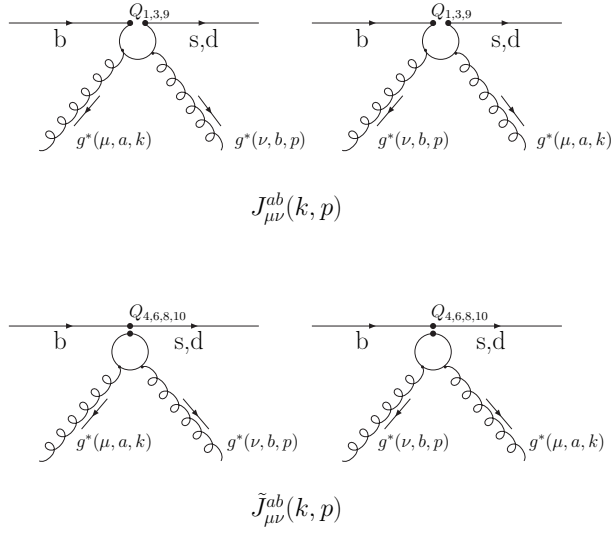


Figure 8: Building blocks $J_{\mu\nu}^{ab}(k, p)$ (corresponding to contractions of the operators $Q_{1,3,9}$) and $\tilde{J}_{\mu\nu}^{ab}(k, p)$ (corresponding to contractions of the operators $Q_{4,6,8,10}$) for Figs. 6(d) and 6(e).

where the first (second) part is symmetric (antisymmetric) with respect to the color structures of the two off-shell gluons. Here k (p), a (b), and μ (ν) are the momentum, color, and polarization of the off-shell gluons, respectively. Below we refer to the gluon with indices (ν, b, p) as the one connected to the spectator quark.

In the NDR scheme, after performing the (shifted) loop momentum integration, we can represent the quantities $T_{\mu\nu}^{\pm}(k, p)$ and $\tilde{T}_{\mu\nu}^{\pm}(k, p)$ as [16, 17]

$$T_{\mu\nu}^+(k, p) = \frac{\alpha_s}{4\pi} \left[E(\mu, \nu, k) \Delta i_5 + E(\mu, \nu, p) \Delta i_6 - E(\mu, k, p) \frac{k_\nu}{k \cdot p} \Delta i_{23} - E(\mu, k, p) \frac{p_\nu}{k \cdot p} \Delta i_{24} - E(\nu, k, p) \frac{k_\mu}{k \cdot p} \Delta i_{25} - E(\nu, k, p) \frac{p_\mu}{k \cdot p} \Delta i_{26} \right] L, \quad (22)$$

$$T_{\mu\nu}^-(k, p) = \frac{\alpha_s}{4\pi} \left[\not{k} g_{\mu\nu} \Delta i_2 + \not{p} g_{\mu\nu} \Delta i_3 + \gamma_\mu k_\nu \Delta i_8 + \gamma_\mu p_\nu \Delta i_9 + \gamma_\nu k_\mu \Delta i_{11} + \gamma_\nu p_\mu \Delta i_{12} + \not{k} \frac{k_\mu k_\nu}{k \cdot p} \Delta i_{15} + \not{k} \frac{k_\mu p_\nu}{k \cdot p} \Delta i_{16} + \not{k} \frac{p_\mu k_\nu}{k \cdot p} \Delta i_{17} + \not{k} \frac{p_\mu p_\nu}{k \cdot p} \Delta i_{18} + \not{p} \frac{k_\mu k_\nu}{k \cdot p} \Delta i_{19} + \not{p} \frac{k_\mu p_\nu}{k \cdot p} \Delta i_{20} + \not{p} \frac{p_\mu k_\nu}{k \cdot p} \Delta i_{21} + \not{p} \frac{p_\mu p_\nu}{k \cdot p} \Delta i_{22} \right] L, \quad (23)$$

$$\tilde{T}_{\mu\nu}^+(k, p) = a T_{\mu\nu}^+(k, p), \quad (24)$$

$$\tilde{T}_{\mu\nu}^-(k, p) = T_{\mu\nu}^-(k, p) + \frac{\alpha_s}{4\pi} \left[\not{k} g_{\mu\nu} \frac{4}{3} - \not{p} g_{\mu\nu} \frac{4}{3} - \gamma_\mu k_\nu \frac{8}{3} - \gamma_\mu p_\nu \frac{4}{3} + \gamma_\nu k_\mu \frac{4}{3} + \gamma_\nu p_\mu \frac{8}{3} \right] L, \quad (25)$$

where $L = 1 - \gamma_5$, and the matrix E in Eq. (22) is defined by

$$\begin{aligned} E(\mu, \nu, k) &= \gamma_\mu \gamma_\nu \not{k} - \gamma_\mu k_\nu + \gamma_\nu k_\mu - \not{k} g_{\mu\nu} \\ &= -i \epsilon_{\mu\nu\alpha\beta} k^\alpha \gamma^\beta \gamma_5, \end{aligned} \quad (26)$$

with the second line obtained in a four dimensional context using the Bjorken-Drell conventions. The parameter a in Eq. (24) denotes the chiral structure of the four-quark operators in the weak vertex with $a = \pm$ corresponding to $(V - A) \otimes (V \mp A)$, respectively. Explicit expressions for the dimensionally regularized Δ_i functions can be found in Appendix B of Ref. [13].

Equipped with these building blocks, we can now evaluate all the Feynman diagrams in Fig. 6. After direct calculations, the final results of these penguin contractions of spectator-scattering amplitudes for hadronic charmless $B \rightarrow PV$ decays can be expressed as

$$\begin{aligned} \mathcal{A}_{Q_1} &= -i \frac{\alpha_s^2 f_B f_{M_1} f_{M_2}}{N_c^3} \lambda_p^{(\prime)} \int_0^1 d\xi \frac{\Phi_1^B(\xi)}{\xi} \int_0^1 dudv \left\{ \left[\frac{2}{3} - \frac{4}{3} \ln \frac{\mu}{m_b} - G(s_p, \bar{u}) \right] f_1(u, v) \right. \\ &\quad \left. + \left[\frac{2}{3} - \frac{4}{3} \ln \frac{\mu}{m_b} - G(s_p, \bar{u}v) \right] f_2(u, v) + f_1(u, v, m_p) \right\}, \end{aligned} \quad (27)$$

$$\begin{aligned} \mathcal{A}_{Q_3} &= i \frac{\alpha_s^2 f_B f_{M_1} f_{M_2}}{N_c^3} \lambda_t^{(\prime)} \int_0^1 d\xi \frac{\Phi_1^B(\xi)}{\xi} \int_0^1 dudv \left\{ [f_1(u, v, 0) + f_1(u, v, 1)] \right. \\ &\quad \left. + \left[\frac{4}{3} - \frac{8}{3} \ln \frac{\mu}{m_b} - G(0, \bar{u}) - G(1, \bar{u}) \right] f_1(u, v) \right. \\ &\quad \left. + \left[\frac{4}{3} - \frac{8}{3} \ln \frac{\mu}{m_b} - G(0, \bar{u}v) - G(1, \bar{u}v) \right] f_2(u, v) \right\}, \end{aligned} \quad (28)$$

$$\mathcal{A}_{Q_9} = -\frac{1}{2} \mathcal{A}_{Q_3}, \quad (29)$$

$$\begin{aligned} \mathcal{A}_{Q_4} &= i \frac{\alpha_s^2 f_B f_{M_1} f_{M_2}}{N_c^3} \lambda_t^{(\prime)} \int_0^1 d\xi \frac{\Phi_1^B(\xi)}{\xi} \int_0^1 dudv \left\{ [(n_f - 2) f_2(u, v, 0) + f_2(u, v, m_c) \right. \\ &\quad \left. + f_2(u, v, m_b)] + \left[-\frac{4n_f}{3} \ln \frac{\mu}{m_b} - (n_f - 2) G(0, \bar{u}) - G(s_c, \bar{u}) - G(1, \bar{u}) \right] f_1(u, v) \right. \\ &\quad \left. + \left[-\frac{4n_f}{3} \ln \frac{\mu}{m_b} - (n_f - 2) G(0, \bar{u}v) - G(s_c, \bar{u}v) - G(1, \bar{u}v) \right] f_2(u, v) \right\}, \end{aligned} \quad (30)$$

$$\begin{aligned} \mathcal{A}_{Q_6} &= i \frac{\alpha_s^2 f_B f_{M_1} f_{M_2}}{N_c^3} \lambda_t^{(\prime)} \int_0^1 d\xi \frac{\Phi_1^B(\xi)}{\xi} \int_0^1 dudv \left\{ [(n_f - 2) f_3(u, v, 0) + f_3(u, v, m_c) \right. \\ &\quad \left. + f_3(u, v, m_b)] + \left[-\frac{4n_f}{3} \ln \frac{\mu}{m_b} - (n_f - 2) G(0, \bar{u}) - G(s_c, \bar{u}) - G(1, \bar{u}) \right] f_1(u, v) \right. \\ &\quad \left. + \left[-\frac{4n_f}{3} \ln \frac{\mu}{m_b} - (n_f - 2) G(0, \bar{u}v) - G(s_c, \bar{u}v) - G(1, \bar{u}v) \right] f_2(u, v) \right\}, \end{aligned} \quad (31)$$

$$\begin{aligned} \mathcal{A}_{Q_8} &= i \frac{\alpha_s^2 f_B f_{M_1} f_{M_2}}{N_c^3} \lambda_t^{(\prime)} \int_0^1 d\xi \frac{\Phi_1^B(\xi)}{\xi} \int_0^1 dudv \left\{ \left[f_3(u, v, m_c) - \frac{1}{2} f_3(u, v, m_b) \right] \right. \\ &\quad \left. + \left[-\frac{2}{3} \ln \frac{\mu}{m_b} - G(s_c, \bar{u}) + \frac{1}{2} G(1, \bar{u}) \right] f_1(u, v) \right\} \end{aligned}$$

$$+ \left[-\frac{2}{3} \ln \frac{\mu}{m_b} - G(s_c, \bar{u}v) + \frac{1}{2} G(1, \bar{u}v) \right] f_2(u, v) \Big\}, \quad (32)$$

$$\begin{aligned} \mathcal{A}_{Q_{10}} = & i \frac{\alpha_s^2 f_B f_{M_1} f_{M_2}}{N_c^3} \lambda_i^{(\nu)} \int_0^1 d\xi \frac{\Phi_1^B(\xi)}{\xi} \int_0^1 dudv \left\{ \left[f_2(u, v, m_c) - \frac{1}{2} f_2(u, v, m_b) \right] \right. \\ & + \left[-\frac{2}{3} \ln \frac{\mu}{m_b} - G(s_c, \bar{u}) + \frac{1}{2} G(1, \bar{u}) \right] f_1(u, v) \\ & \left. + \left[-\frac{2}{3} \ln \frac{\mu}{m_b} - G(s_c, \bar{u}v) + \frac{1}{2} G(1, \bar{u}v) \right] f_2(u, v) \right\}, \quad (33) \end{aligned}$$

with the subscript Q_i denoting the contraction of Q_i operator in the weak vertex, and

$$\begin{aligned} f_1(u, v) = & \Phi_{M_2}(u) \Phi_{M_1}(v) \left[\frac{2u + v - 3}{12(1-u)(1-v)^2} + \frac{3(2u + v - 3)}{4(1-u)(1-v)v} \right] \\ & + r_\chi^{M_1} \Phi_{M_2}(u) \Phi_{m_1}(v) \left[\frac{3(v-3)}{4(1-u)(1-v)v} - \frac{1}{12(1-u)(1-v)} \right] \\ & + r_\chi^{M_1} r_\chi^{M_2} \Phi_{m_2}(u) \Phi_{m_1}(v) \left[\frac{2u-1}{12(1-u)(1-v)} + \frac{3(2u+v-2uv-3)}{4(1-u)(1-v)v} \right] \\ & + r_\chi^{M_2} \Phi_{m_2}(u) \Phi_{M_1}(v) \left[\frac{v-3}{12(1-v)^2} + \frac{3(v-3)}{4(1-v)v} \right], \quad (34) \end{aligned}$$

$$\begin{aligned} f_2(u, v) = & \Phi_{M_2}(u) \Phi_{M_1}(v) \frac{1}{6(1-v)^2} - r_\chi^{M_1} \Phi_{M_2}(u) \Phi_{m_1}(v) \frac{1}{6u(1-v)} \\ & + r_\chi^{M_1} r_\chi^{M_2} \Phi_{m_2}(u) \Phi_{m_1}(v) \frac{1}{6(1-v)} + r_\chi^{M_2} \Phi_{m_2}(u) \Phi_{M_1}(v) \frac{1}{6(1-v)^2}, \quad (35) \end{aligned}$$

$$\begin{aligned} f_1(u, v, m_q) = & \Phi_{M_2}(u) \Phi_{M_1}(v) \left[\frac{3\Delta i_2}{8(1-u)(1-v)} + \frac{3\Delta i_3}{8(1-u)v} + \frac{7\Delta i_6}{24(1-u)v} \right. \\ & \left. + \frac{3\Delta i_8}{8(1-v)v} + \frac{7\Delta i_{23}}{24(1-v)v} + \frac{7(1-u+v)\Delta i_5}{24(1-u)(1-v)v} \right] \\ & - r_\chi^{M_1} \Phi_{M_2}(u) \Phi_{m_1}(v) \left[\frac{7\Delta i_5}{12(1-u)(1-v)} + \frac{3(\Delta i_2 - \Delta i_8 + \Delta i_{17})}{8(1-u)(1-v)} \right. \\ & \left. + \frac{7(\Delta i_6 + \Delta i_{26})}{24(1-u)v} + \frac{3(\Delta i_3 + 2\Delta i_{12} + \Delta i_{21})}{8(1-u)v} \right] \\ & + r_\chi^{M_1} r_\chi^{M_2} \Phi_{m_2}(u) \Phi_{m_1}(v) \left[\frac{7\Delta i_5}{12(1-v)} + \frac{3(\Delta i_2 + \Delta i_8 - \Delta i_{12} + \Delta i_{17})}{8v} \right. \\ & \left. - \frac{7u\Delta i_{23}}{12(1-u)(1-v)} + \frac{3(\Delta i_2 + \Delta i_8 + \Delta i_{17})}{8(1-u)(1-v)} + \frac{3u(\Delta i_3 + \Delta i_{21})}{8(1-u)v} \right. \\ & \left. + \frac{7(\Delta i_6 + \Delta i_{26})}{24(1-u)v} \right] \\ & - r_\chi^{M_2} \Phi_{m_2}(u) \Phi_{M_1}(v) \left[\frac{3(\Delta i_2 - \Delta i_8)}{8(1-v)v} + \frac{7(\Delta i_{23} + 2\Delta i_5)}{24(1-v)v} \right], \quad (36) \end{aligned}$$

$$f_{2,(3)}(u, v, m_q) = \Phi_{M_2}(u) \Phi_{M_1}(v) \left[-\frac{(3-2u-2v)}{2(1-u)(1-v)v} + \frac{3\Delta i_2}{8(1-u)(1-v)} + \frac{3\Delta i_3}{8(1-u)v} \right]$$

$$\begin{aligned}
& \left[\pm \frac{7 \Delta i_6}{24(1-u)v} + \frac{3 \Delta i_8}{8(1-v)v} \pm \frac{7 \Delta i_{23}}{24(1-v)v} \pm \frac{7(1-u+v) \Delta i_5}{24(1-u)(1-v)v} \right] \\
- & r_\chi^{M_1} \Phi_{M_2}(u) \Phi_{m_1}(v) \left[\frac{3}{2(1-u)(1-v)v} + \frac{3(\Delta i_3 + 2 \Delta i_{12} + \Delta i_{21})}{8(1-u)v} \right. \\
& \left. \pm \frac{7(\Delta i_6 + \Delta i_{26})}{24(1-u)v} \pm \frac{7 \Delta i_5}{12(1-u)(1-v)} + \frac{3(\Delta i_2 - \Delta i_8 + \Delta i_{17})}{8(1-u)(1-v)} \right] \\
+ & r_\chi^{M_1} r_\chi^{M_2} \Phi_{m_2}(u) \Phi_{m_1}(v) \left[-\frac{3-2u-2v+2uv}{2(1-u)(1-v)v} \mp \frac{7u \Delta i_{23}}{12(1-u)(1-v)} \right. \\
& \left. \pm \frac{7 \Delta i_5}{12(1-v)} + \frac{3u(\Delta i_3 + \Delta i_{21})}{8(1-u)v} \pm \frac{7(\Delta i_6 + \Delta i_{26})}{24(1-u)v} \right. \\
& \left. + \frac{3(\Delta i_2 + \Delta i_8 + \Delta i_{17})}{8(1-u)(1-v)} + \frac{3(\Delta i_2 + \Delta i_8 - \Delta i_{12} + \Delta i_{17})}{8v} \right] \\
- & r_\chi^{M_2} \Phi_{m_2}(u) \Phi_{M_1}(v) \left[\frac{3}{2(1-v)v} + \frac{3(\Delta i_2 - \Delta i_8)}{8(1-v)v} \pm \frac{7(\Delta i_{23} + 2 \Delta i_5)}{24(1-v)v} \right] \quad (37)
\end{aligned}$$

when M_1 is a pseudoscalar and M_2 a vector meson. For the opposite case, i.e., M_1 is a vector and M_2 a pseudoscalar meson, one needs only change the signs of the last two terms in the functions f_i defined above. At this stage, the Δ_i functions appearing in Eqs. (36) and (37) are the ones that have been performed the Feynman parameter integrals, whose explicit expressions can be found in Appendix B of Refs. [13, 19]. For convenience, we also list them in Appendix A.

With the individual operator contribution given above, the total contributions of the penguin contractions of spectator-scattering amplitudes can be written as

$$\begin{aligned}
\mathcal{A}'(B \rightarrow PV) = & \frac{G_F}{\sqrt{2}} \left[\sum_{p=u,c} C_1 \mathcal{A}_{Q_1} + (C_3 - \frac{1}{2} C_9) \mathcal{A}_{Q_3} + C_4 \mathcal{A}_{Q_4} + C_6 \mathcal{A}_{Q_6} \right. \\
& \left. + C_8 \mathcal{A}_{Q_8} + C_{10} \mathcal{A}_{Q_{10}} + C_{8g}^{\text{eff}} \mathcal{A}_{Q_{8g}} \right], \quad (38)
\end{aligned}$$

where the superscript ' \prime ' indicates the one to be distinguished from the next-to-leading order results given by Eqs. (8) and (12). The total decay amplitude is then given as

$$\langle PV | \mathcal{H}_{\text{eff}} | B \rangle = \mathcal{A}(B \rightarrow PV) + \mathcal{A}^{\text{ann}}(B \rightarrow PV) + \mathcal{A}'(B \rightarrow PV). \quad (39)$$

3 Numerical results and discussions

With the theoretical expressions given above and the input parameters collected in Appendix B, we can now evaluate the branching ratios and CP -violating asymmetries for two-body hadronic

charmless $B \rightarrow PV$ decays, with $P = (\pi, K)$ and $V = (\rho, \omega, K^*, \phi)$. For each quantity, we first give the results at next-to-leading order in α_s , and then take into account the higher order penguin contractions of spectator-scattering amplitudes induced by the $b \rightarrow Dg^*g^*$ transitions. The combined contributions of these two pieces, denoted by $\mathcal{O}(\alpha_s + \alpha_s^2)$, are then given in the last. For comparison, results based on the NF approximation are also presented. All the experimental data are taken from the home page of the Heavy Flavor Averaging Group (HFAG) [26].

In order to show the renormalization scale dependence of the branching ratios and CP asymmetries, we give results of two cases for each decay mode with the first one evaluated at the scale $\mu = m_b$, while the second at the scale $\mu = m_b/2$. In addition, our calculations depend on many input parameters, which cause quite large theoretical uncertainties. We will consider the main theoretical uncertainties arising from the strange-quark mass (with the ratio m_q/m_s fixed, all chiral enhancement factors r_χ^P depend on this mass), CKM matrix elements, form factors, and the first inverse moment of the B -meson distribution amplitude λ_B .²

3.1 Numerical analysis of penguin contractions of spectator-scattering amplitudes

Before presenting numerical results for branching ratios and CP asymmetries, we would discuss the relative strength of each Feynman diagram shown in Figs. 5 and 6. For convenience, we denote the decay modes with the pseudoscalar meson picking up the spectator quark by $B \rightarrow PV$, while for the vector meson picking up the spectator quark by $B \rightarrow VP$.

Firstly, we study the relative strength of the three Feynman diagrams shown in Fig. 5. Since contributions of these diagrams are all proportional to

$$S_1 = -i \frac{\alpha_s^2 f_B f_{M_1} f_{M_2}}{N_c^3} \lambda_t^{(\prime)} \int_0^1 d\xi \frac{\Phi_1^B(\xi)}{\xi}, \quad (40)$$

we have factorized S_1 out off the numerical results shown in Table 1.

From the numerical results for the dipole operator Q_{8g} contractions given in Table 1, we

²Since the theoretical uncertainties coming from the weak annihilation and twist-3 hard-spectator interaction contributions (parameterized by the quantities X_H and X_A) are already known to be quite large[12], we do not consider these uncertainties here and simply use the default values given by $X_{H(A)} = \log m_B/\lambda_h$ as specified in Appendix B. Uncertainties coming from the other input parameters are generally small and have been neglected.

Table 1: Numerical results of each Feynman diagram shown in Fig. 5 with the asymptotic forms of the meson LCDAs. Terms involving the twist-three LCDAs are given in unit of the factor r_χ^M defined by Eq. (11). The subscripts $M_1 = P(V)$ and $M_2 = V(P)$ for the $B \rightarrow PV$ ($B \rightarrow VP$) rows. The same for $m_{1,2}$.

	Decay mode	$\Phi_{M_2}\Phi_{M_1}$	$\Phi_{M_2}\Phi_{m_1}$	$\Phi_{m_2}\Phi_{M_1}$	$\Phi_{m_2}\Phi_{m_1}$
Fig. 5(a)	$B \rightarrow PV$	-67.50	-125.76	-9.64	-18.94
	$B \rightarrow VP$	-67.50	4.82	34.71	-3.79
Figs. 5(b+c)	$B \rightarrow PV$	-1.50	-3.54	-1.07	-0.42
	$B \rightarrow VP$	-1.50	-1.61	1.86	0.42

can see that the main contributions come from Fig. 5(a), and the other ones play only a minor role. It is also noted that these amplitudes do not have strong phases.

To analyze strong phase sources and the relative strength of the individual Feynman diagram shown in Fig. 6, we study the Q_1^c contraction in the weak vertex. The contribution of each Feynman diagram is proportional to

$$S_2 = i \frac{\alpha_s^2 f_B f_{M_1} f_{M_2}}{N_c^3} \lambda_c^{(i)} \int_0^1 d\xi \frac{\Phi_1^B(\xi)}{\xi}, \quad (41)$$

which has also been factorized out. The numerical results given in Table 2 are independent of S_2 .

From the numerical results given in Table 2, we have the following observations: (i) contributions of Figs. 6(b) and 6(c) are generally much smaller than those of the other three ones, and the main contributions come from the diagrams Figs. 6(d) and 6(e); (ii) although each term labelled by the meson LCDAs in each Feynman diagram has a large imaginary part, and hence a large strong phase, the total strong phase of each Feynman diagram is small due to cancellations among the four terms. (iii) for each term labelled by the same LCDAs, there also exist cancellations between the contributions of the diagrams Fig. 6(a) and Figs. 6(d+e).

Thus the total strong phase is found to be quite small after summing all the five diagrams shown in Fig. 6. Moreover, the cancellation does not depend on the parameters in S_2 .

Table 2: Numerical results of each Feynman diagram shown in Fig. 6. Others are the same as Table 1.

	modes	$\Phi_{M_2}\Phi_{M_1}$	$\Phi_{M_2}\Phi_{m_1}$	$\Phi_{m_2}\Phi_{M_1}$	$\Phi_{m_2}\Phi_{m_1}$
Fig. 6(a)	PV	$-1.39 - 12.65 i$	$0.17 - 14.10 i$	$-0.15 + 15.38 i$	$0.12 + 13.51 i$
	VP	$-1.39 - 12.65 i$	$-0.02 + 1.28 i$	$-0.12 + 11.11 i$	$-0.01 - 0.44 i$
Figs. 6(b+c)	PV	$-0.01 - 1.05 i$	$-0.12 - 1.21 i$	$-0.62 + 0.81 i$	$-0.18 - 0.11 i$
	VP	$-0.01 - 1.05 i$	$-0.39 - 1.25 i$	$-0.08 + 0.78 i$	$-0.10 - 0.19 i$
Figs. 6(d+e)	PV	$-9.03 + 14.94 i$	$19.19 + 28.30 i$	$4.32 - 21.29 i$	$10.82 - 15.69 i$
	VP	$-9.03 + 14.94 i$	$14.26 + 9.04 i$	$0.83 - 16.78 i$	$-0.39 - 3.46 i$

3.2 Branching ratios of $B \rightarrow PV$ decays

In the following discussions, we classify the two-body hadronic charmless $B \rightarrow PV$ decays into two categories: the strange-conserving ($\Delta S = 0$) and the strange-changing ($\Delta S = 1$) processes. The higher order penguin contractions of spectator-scattering amplitudes are expected to have more significant impacts on the $\Delta S = 1$ processes than on the $\Delta S = 0$ ones, due to the CKM factor suppressions in the latter.

Numerical results of the CP -averaged branching ratios for these decays are collected in Tables 3, 4, and 5, where the theoretical error bars are due to the uncertainties of the input parameters CKM elements, quark masses, transition form factors, and λ_B as collected in Appendix B. Generally, the theoretical uncertainties are quite large, which are larger than $\mathcal{O}(\alpha_s^2)$ corrections for tree-dominated decay modes, but comparable for strong penguin-dominated decay modes. For most decay modes, the α_s^2 corrections reduce the renormalization scale dependence of the theoretical predictions.

For $\Delta S = 0$ decays, since the $b \rightarrow d$ penguin amplitudes are suppressed by the CKM factor λ_t' compared to the $b \rightarrow s$ penguin amplitudes, most of them are expected to be dominated by the tree amplitudes, however with a few exceptions. From the numerical results given in Tables 3 and 4, we have the following general remarks:

- The decays $\overline{B}^0 \rightarrow \pi^\pm \rho^\mp$ and $B^- \rightarrow \pi^0 \rho^-, \pi^- \rho^0, \pi^- \omega$. Our results are generally consistent

Table 3: CP -averaged branching ratios (in units of 10^{-6}) of tree-dominated $B \rightarrow PV$ decays with $\Delta S = 0$. $\bar{\mathcal{B}}^f$ and $\bar{\mathcal{B}}^{f+a}$ denote the results without and with the annihilation contributions, respectively. Results in columns $\mathcal{O}(\alpha_s + \alpha_s^2)$ are the ones with the higher order penguin contraction contributions included. For each decay mode, the first row is evaluated at the scale $\mu = m_b$, while the second one at the scale $\mu = m_b/2$. The theoretical errors correspond to the uncertainties of the input parameters collected in Appendix B. The NF results are also shown for comparison.

Decay mode	NF	$\bar{\mathcal{B}}^f$		$\bar{\mathcal{B}}^{f+a}$		EXP.
		$\mathcal{O}(\alpha_s)$	$\mathcal{O}(\alpha_s + \alpha_s^2)$	$\mathcal{O}(\alpha_s)$	$\mathcal{O}(\alpha_s + \alpha_s^2)$	
$B^- \rightarrow \pi^- \rho^0$	$8.76^{+3.56}_{-2.93}$	$8.15^{+3.69}_{-2.86}$	$8.02^{+3.77}_{-2.80}$	$8.13^{+3.53}_{-2.63}$	$8.01^{+3.73}_{-2.58}$	$8.7^{+1.0}_{-1.1}$
	$7.52^{+3.36}_{-2.45}$	$7.45^{+3.42}_{-2.57}$	$7.36^{+3.71}_{-2.67}$	$7.44^{+3.25}_{-2.59}$	$7.36^{+3.60}_{-2.46}$	
$B^- \rightarrow \pi^0 \rho^-$	$13.91^{+6.21}_{-4.87}$	$13.05^{+6.32}_{-4.53}$	$13.31^{+6.06}_{-4.76}$	$13.22^{+5.94}_{-4.80}$	$13.48^{+6.79}_{-5.05}$	$10.8^{+1.4}_{-1.5}$
	$13.08^{+6.21}_{-4.54}$	$12.82^{+6.32}_{-4.86}$	$13.01^{+6.81}_{-5.16}$	$13.00^{+5.99}_{-4.94}$	$13.20^{+6.12}_{-4.89}$	
$\bar{B}^0 \rightarrow \pi^+ \rho^-$	$19.78^{+9.88}_{-7.28}$	$19.37^{+9.25}_{-7.62}$	$19.73^{+10.46}_{-7.28}$	$20.34^{+10.20}_{-7.95}$	$20.72^{+9.94}_{-7.85}$	$13.9^{+2.2}_{-2.1}$
	$20.82^{+10.64}_{-7.83}$	$20.22^{+11.10}_{-8.11}$	$20.48^{+11.71}_{-7.65}$	$21.25^{+11.03}_{-8.26}$	$21.52^{+10.22}_{-7.86}$	
$\bar{B}^0 \rightarrow \pi^- \rho^+$	$10.72^{+4.61}_{-3.68}$	$10.51^{+4.69}_{-3.55}$	$10.47^{+4.60}_{-3.49}$	$11.15^{+4.71}_{-3.82}$	$11.11^{+4.99}_{-3.75}$	$10.1^{+2.1}_{-1.9}$
	$11.18^{+5.08}_{-3.74}$	$10.90^{+4.71}_{-3.89}$	$10.86^{+4.87}_{-3.92}$	$11.57^{+5.23}_{-4.02}$	$11.52^{+4.99}_{-3.90}$	
$\bar{B}^0 \rightarrow \pi^\pm \rho^\mp$	$30.50^{+13.65}_{-10.39}$	$29.88^{+13.22}_{-10.18}$	$30.20^{+13.85}_{-10.52}$	$31.49^{+13.04}_{-10.64}$	$31.83^{+13.82}_{-11.48}$	24.0 ± 2.5
	$32.00^{+14.58}_{-11.12}$	$31.12^{+14.60}_{-10.56}$	$31.34^{+13.82}_{-11.58}$	$32.82^{+14.96}_{-11.82}$	$33.04^{+16.32}_{-11.01}$	
$\bar{B}^0 \rightarrow \pi^0 \rho^0$	$0.47^{+0.20}_{-0.15}$	$0.40^{+0.35}_{-0.18}$	$0.39^{+0.33}_{-0.15}$	$0.30^{+0.29}_{-0.13}$	$0.30^{+0.27}_{-0.13}$	$1.83^{+0.56}_{-0.55}$
	$0.13^{+0.06}_{-0.04}$	$0.29^{+0.23}_{-0.12}$	$0.29^{+0.24}_{-0.11}$	$0.22^{+0.19}_{-0.08}$	$0.23^{+0.20}_{-0.09}$	
$B^- \rightarrow \pi^- \omega$	$7.87^{+3.61}_{-2.57}$	$7.36^{+3.50}_{-2.44}$	$7.47^{+3.80}_{-2.53}$	$7.10^{+3.43}_{-2.62}$	$7.21^{+3.21}_{-2.37}$	6.6 ± 0.6
	$6.96^{+2.94}_{-2.28}$	$6.84^{+3.08}_{-2.39}$	$6.90^{+3.38}_{-2.31}$	$6.54^{+2.89}_{-2.23}$	$6.60^{+3.29}_{-2.28}$	
$\bar{B}^0 \rightarrow \pi^0 \omega$	$0.01^{+0.03}_{-0.01}$	$0.02^{+0.03}_{-0.01}$	$0.02^{+0.03}_{-0.01}$	$0.005^{+0.015}_{-0.003}$	$0.004^{+0.014}_{-0.003}$	< 1.2
	$0.03^{+0.04}_{-0.02}$	$0.02^{+0.02}_{-0.01}$	$0.02^{+0.03}_{-0.01}$	$0.010^{+0.018}_{-0.007}$	$0.010^{+0.020}_{-0.007}$	

with the experimental data within errors. Since these decay channels are dominated by the color-allowed tree amplitudes, both the weak annihilation and the higher order penguin contraction contributions are small. In addition, the main theoretical errors come

Table 4: CP -averaged branching ratios (in units of 10^{-6}) of penguin-dominated (the upper six) and annihilation-dominated (the last two) $B \rightarrow PV$ decays with $\Delta S = 0$. The captions are the same as Table 3.

Decay mode	NF	$\bar{\mathcal{B}}^f$		$\bar{\mathcal{B}}^{f+a}$		EXP.
		$\mathcal{O}(\alpha_s)$	$\mathcal{O}(\alpha_s + \alpha_s^2)$	$\mathcal{O}(\alpha_s)$	$\mathcal{O}(\alpha_s + \alpha_s^2)$	
$B^- \rightarrow K^- K^{*0}$	$0.15^{+0.07}_{-0.04}$	$0.18^{+0.08}_{-0.07}$	$0.28^{+0.14}_{-0.09}$	$0.23^{+0.11}_{-0.09}$	$0.34^{+0.16}_{-0.11}$	< 5.3
	$0.32^{+0.13}_{-0.11}$	$0.23^{+0.10}_{-0.08}$	$0.33^{+0.15}_{-0.10}$	$0.29^{+0.14}_{-0.10}$	$0.40^{+0.20}_{-0.13}$	
$\bar{B}^0 \rightarrow \bar{K}^0 K^{*0}$	$0.14^{+0.06}_{-0.04}$	$0.16^{+0.09}_{-0.06}$	$0.26^{+0.12}_{-0.08}$	$0.20^{+0.10}_{-0.07}$	$0.31^{+0.15}_{-0.10}$...
	$0.29^{+0.14}_{-0.09}$	$0.22^{+0.10}_{-0.08}$	$0.31^{+0.15}_{-0.10}$	$0.26^{+0.10}_{-0.09}$	$0.36^{+0.16}_{-0.11}$	
$B^- \rightarrow K^0 K^{*-}$	$0.06^{+0.13}_{-0.04}$	$0.10^{+0.21}_{-0.07}$	$0.10^{+0.20}_{-0.07}$	$0.18^{+0.27}_{-0.10}$	$0.18^{+0.26}_{-0.10}$...
	$0.05^{+0.14}_{-0.04}$	$0.08^{+0.18}_{-0.06}$	$0.07^{+0.17}_{-0.05}$	$0.15^{+0.25}_{-0.09}$	$0.14^{+0.23}_{-0.08}$	
$\bar{B}^0 \rightarrow K^0 \bar{K}^{*0}$	$0.06^{+0.12}_{-0.04}$	$0.09^{+0.19}_{-0.06}$	$0.09^{+0.18}_{-0.06}$	$0.18^{+0.26}_{-0.10}$	$0.17^{+0.27}_{-0.09}$...
	$0.04^{+0.14}_{-0.03}$	$0.07^{+0.16}_{-0.05}$	$0.06^{+0.15}_{-0.04}$	$0.15^{+0.25}_{-0.08}$	$0.14^{+0.24}_{-0.08}$	
$B^- \rightarrow \pi^- \phi$	≈ 0.001	≈ 0.008	< 0.41
	≈ 0.001	≈ 0.007	
$\bar{B}^0 \rightarrow \pi^0 \phi$	≈ 0.0003	≈ 0.004	< 1.0
	≈ 0.0003	≈ 0.003	
$\bar{B}^0 \rightarrow K^{*-} K^+$	$0.018^{+0.004}_{-0.004}$
	$0.019^{+0.005}_{-0.004}$
$\bar{B}^0 \rightarrow K^- K^{*+}$	$0.018^{+0.004}_{-0.004}$
	$0.019^{+0.005}_{-0.004}$

from the uncertainties of the form factors and CKM matrix elements.

- The decays $\bar{B}^0 \rightarrow \pi^0 \rho^0$ and $\bar{B}^0 \rightarrow \pi^0 \omega$. Since these decay channels are dominated by the color-suppressed tree amplitudes, their branching ratios are predicted to be very small. The higher order penguin contraction contributions are always much smaller than the weak annihilation contributions. Besides the form factors and CKM matrix elements, the spectator-scattering amplitudes also cause sizable uncertainties to their CP -averaged branching ratios.

Table 5: CP -averaged branching ratios (in units of 10^{-6}) of penguin-dominated $B \rightarrow PV$ decays with $\Delta S = 1$. The captions are the same as Table 3.

Decay mode	NF	$\bar{\mathcal{B}}^f$		$\bar{\mathcal{B}}^{f+a}$		EXP.
		$\mathcal{O}(\alpha_s)$	$\mathcal{O}(\alpha_s + \alpha_s^2)$	$\mathcal{O}(\alpha_s)$	$\mathcal{O}(\alpha_s + \alpha_s^2)$	
$B^- \rightarrow \pi^- \bar{K}^{*0}$	$2.37^{+0.72}_{-0.64}$	$2.60^{+0.95}_{-0.88}$	$4.26^{+1.72}_{-1.21}$	$3.50^{+1.22}_{-1.04}$	$5.39^{+2.01}_{-1.44}$	10.8 ± 0.8
	$4.89^{+1.46}_{-1.28}$	$3.35^{+1.27}_{-1.13}$	$5.01^{+1.81}_{-1.41}$	$4.45^{+1.51}_{-1.36}$	$6.34^{+2.18}_{-1.70}$	
$B^- \rightarrow \pi^0 K^{*-}$	$1.82^{+0.76}_{-0.54}$	$1.88^{+0.79}_{-0.56}$	$2.73^{+1.23}_{-0.81}$	$2.33^{+0.96}_{-0.69}$	$3.29^{+1.31}_{-0.89}$	6.9 ± 2.3
	$3.03^{+1.15}_{-0.88}$	$2.21^{+0.87}_{-0.74}$	$3.05^{+1.25}_{-0.89}$	$2.75^{+1.08}_{-0.79}$	$3.70^{+1.36}_{-1.01}$	
$\bar{B}^0 \rightarrow \pi^+ K^{*-}$	$1.84^{+0.90}_{-0.67}$	$1.92^{+0.89}_{-0.72}$	$3.04^{+1.64}_{-1.04}$	$2.47^{+1.08}_{-0.82}$	$3.78^{+1.84}_{-1.34}$	$11.7^{+1.5}_{-1.4}$
	$3.40^{+1.49}_{-1.11}$	$2.32^{+1.12}_{-0.84}$	$3.43^{+1.67}_{-1.13}$	$2.99^{+1.31}_{-0.96}$	$4.30^{+2.09}_{-1.44}$	
$\bar{B}^0 \rightarrow \pi^0 \bar{K}^{*0}$	$0.49^{+0.27}_{-0.20}$	$0.53^{+0.35}_{-0.26}$	$1.08^{+0.77}_{-0.46}$	$0.80^{+0.42}_{-0.33}$	$1.45^{+0.86}_{-0.56}$	1.7 ± 0.8
	$1.24^{+0.56}_{-0.46}$	$0.73^{+0.50}_{-0.35}$	$1.28^{+0.73}_{-0.50}$	$1.07^{+0.56}_{-0.43}$	$1.72^{+0.91}_{-0.65}$	
$B^- \rightarrow K^- \phi$	$3.71^{+1.18}_{-1.00}$	$2.73^{+1.33}_{-1.20}$	$5.06^{+2.01}_{-1.48}$	$4.04^{+1.58}_{-1.48}$	$6.77^{+2.78}_{-1.74}$	$9.03^{+0.65}_{-0.63}$
	$10.17^{+3.21}_{-3.23}$	$3.90^{+1.93}_{-1.69}$	$6.32^{+2.07}_{-1.77}$	$5.59^{+2.23}_{-2.11}$	$8.42^{+2.67}_{-2.22}$	
$\bar{B}^0 \rightarrow \bar{K}^0 \phi$	$3.45^{+1.10}_{-0.93}$	$2.53^{+1.20}_{-1.11}$	$4.70^{+1.86}_{-1.37}$	$3.67^{+1.50}_{-1.37}$	$6.19^{+2.40}_{-1.69}$	$8.3^{+1.2}_{-1.0}$
	$9.46^{+3.01}_{-2.59}$	$3.63^{+1.81}_{-1.61}$	$5.88^{+2.10}_{-1.67}$	$5.09^{+2.10}_{-1.87}$	$7.70^{+2.55}_{-2.14}$	
$B^- \rightarrow \bar{K}^0 \rho^-$	$1.05^{+2.12}_{-0.73}$	$1.74^{+3.09}_{-1.16}$	$1.65^{+3.10}_{-1.08}$	$3.18^{+4.42}_{-1.85}$	$3.05^{+3.94}_{-1.73}$	< 48
	$0.76^{+2.17}_{-0.63}$	$1.36^{+2.99}_{-0.97}$	$1.20^{+2.69}_{-0.86}$	$2.73^{+3.77}_{-1.58}$	$2.49^{+3.83}_{-1.47}$	
$B^- \rightarrow K^- \rho^0$	$0.77^{+1.06}_{-0.35}$	$0.99^{+1.70}_{-0.59}$	$0.96^{+1.69}_{-0.56}$	$1.56^{+2.38}_{-0.95}$	$1.51^{+2.24}_{-0.95}$	$4.23^{+0.56}_{-0.57}$
	$0.58^{+1.11}_{-0.26}$	$0.78^{+1.56}_{-0.43}$	$0.72^{+1.35}_{-0.36}$	$1.28^{+2.10}_{-0.78}$	$1.19^{+2.12}_{-0.70}$	
$\bar{B}^0 \rightarrow K^- \rho^+$	$2.50^{+3.17}_{-1.36}$	$3.44^{+4.20}_{-1.91}$	$3.31^{+4.09}_{-1.81}$	$5.27^{+5.29}_{-2.67}$	$5.11^{+5.18}_{-2.55}$	$9.9^{+1.6}_{-1.5}$
	$2.28^{+3.33}_{-1.33}$	$3.04^{+3.66}_{-1.69}$	$2.81^{+3.77}_{-1.54}$	$4.86^{+5.19}_{-2.42}$	$4.55^{+5.00}_{-2.32}$	
$\bar{B}^0 \rightarrow \bar{K}^0 \rho^0$	$1.42^{+1.59}_{-0.72}$	$1.98^{+2.13}_{-1.03}$	$1.90^{+2.12}_{-0.97}$	$3.03^{+3.01}_{-1.35}$	$2.94^{+2.68}_{-1.39}$	5.1 ± 1.6
	$1.32^{+1.79}_{-0.76}$	$1.80^{+2.17}_{-0.94}$	$1.66^{+1.97}_{-0.95}$	$2.88^{+2.61}_{-1.35}$	$2.70^{+2.59}_{-1.27}$	
$B^- \rightarrow K^- \omega$	$0.89^{+1.18}_{-0.48}$	$2.16^{+2.33}_{-1.12}$	$2.10^{+2.55}_{-1.11}$	$3.07^{+3.01}_{-1.49}$	$2.99^{+3.07}_{-1.44}$	6.5 ± 0.6
	$0.40^{+0.87}_{-0.13}$	$1.75^{+2.15}_{-0.97}$	$1.65^{+2.27}_{-0.94}$	$2.61^{+3.20}_{-1.42}$	$2.47^{+3.25}_{-1.29}$	
$\bar{B}^0 \rightarrow \bar{K}^0 \omega$	$0.17^{+0.66}_{-0.15}$	$1.03^{+1.74}_{-0.68}$	$0.99^{+1.67}_{-0.66}$	$1.78^{+2.45}_{-1.00}$	$1.72^{+2.26}_{-0.96}$	4.7 ± 0.6
	$0.03^{+0.29}_{-0.03}$	$0.76^{+1.49}_{-0.52}$	$0.69^{+1.45}_{-0.47}$	$1.43^{+2.16}_{-0.83}$	$1.33^{+2.09}_{-0.82}$	

- The decays $B^- \rightarrow K^- K^{*0}$ and $\bar{B}^0 \rightarrow \bar{K}^0 K^{*0}$. These decay channels are dominated by the $b \rightarrow d$ penguin amplitudes, and the dominant term is proportional to the coefficient $\alpha_4^p(PV)$. Since $\alpha_4^c \approx \alpha_4^u$ and $|\lambda'_u| \approx |\lambda'_c|$, large interference effects between these two terms are expected and the branching ratios of these decay modes have a strong dependence on the weak phase angle $\gamma = \arg(V_{ub}^*)$. The higher order penguin contraction contributions can provide about 60% enhancements to their branching ratios, and are larger than the weak annihilation contributions (which also play an important role in these decay channels). Since the higher order penguin contraction contributions are all involved the quantity λ_B , the main theoretical errors in the CP -averaged branching ratios, besides the CKM matrix elements and form factors, also originate from this quantity.
- The decays $B^- \rightarrow K^0 K^{*-}$ and $\bar{B}^0 \rightarrow K^0 \bar{K}^{*0}$. The dominant contribution to the decay amplitudes is proportional to the coefficient $\alpha_4^p(VP)$, where delicate cancellations between the vector and scalar penguin contributions occur, their branching ratios are therefore predicted to be relatively small. This also renders the weak annihilation contributions potentially large. On the other hand, since these decay channels belong to the category of $B \rightarrow VP$ decays, the higher order penguin contraction contributions are predicted to be small. The theoretical errors in the CP -averaged branching ratios of these decay channels are large, mainly due to the variations of the strange-quark mass and λ_B .
- The decays $B^- \rightarrow \pi^- \phi$ and $\bar{B}^0 \rightarrow \pi^0 \phi$. These two decay channels do not receive the weak annihilation contributions and are electro-weak penguin dominated processes. Due to the small coefficients $\alpha_3^p(\pi\phi)$ and $\alpha_{3,ew}^p(\pi\phi)$, their branching ratios are predicted to be quite small. From the numerical results, we can see that large “nonfactorizable” contributions dominate these decays, while the theoretical predictions are still quite lower than the experimental upper bounds. The higher order penguin contraction contributions have negligible impact on these decay channels.
- The decays $\bar{B}^0 \rightarrow K^+ K^{*-}, K^- K^{*+}$. These two decay channels are pure annihilation processes. Studying on these decay modes may be helpful to learn more about the strength of annihilation contributions and to provide some useful information about final-state interactions. The higher order penguin contraction contributions have no impacts on

these decay channels.

For penguin-dominated $\Delta S = 1$ decays, since the QCD penguin coefficients $\alpha_{3,4}^p$ can receive large “nonfactorizable” contributions within the QCDF formalism, the predicted branching ratios for these decay modes are usually quite different from those obtained with the NF approximation. In addition, the weak annihilation contributions to these decay channels are quite sizable. From the numerical results given in Table 5, we have the following general remarks:

- The decays $B \rightarrow \pi K^*$ and $B \rightarrow K\phi$. With central values of our input parameters, our results are still lower than the experimental data. The dominant contribution to the decay amplitudes is proportional to the coefficient $\alpha_4^p(PV)$. The higher order penguin contraction contributions can give enhancements to these branching ratios by about 40% \sim 90%, and reduce the discrepancies between the theoretical predictions and the experimental data. In addition, large interference effects between the tree and penguin amplitudes in some decay channels, such as $\overline{B}^0 \rightarrow \pi^+ K^{*-}$ and $B^- \rightarrow \pi^0 K^{*-}$, are expected. It is thus possible to gain some information on the weak angle γ from these decay channels. The main theoretical errors are due to the uncertainties of the CKM matrix elements, form factors, and λ_B .
- The decays $B \rightarrow K\rho$ and $B \rightarrow K\omega$. In their decay amplitudes, the dominant term is proportional to the coefficient $\alpha_4^p(VP)$. Because of the destructive interference between the vector and the scalar penguin contributions, the coefficient $\alpha_4^p(VP)$ is reduced to a large extent, making the branching ratios of these decay modes much smaller than those of the corresponding $B \rightarrow PP$ counterparts. It also makes the sub-leading terms, for example, the weak annihilation contributions, very important to account for the experimental data. Since these decay channels also belong to the category of $B \rightarrow VP$ decays, the higher order penguin contraction contributions are quite small, and tend to decrease the NLO results. The main theoretical errors are due to the uncertainties of the strange-quark mass and form factors.

From the above discussions, we can see that the higher order penguin contractions of spectator-scattering amplitudes play an important role in penguin-dominated $B \rightarrow PV$ decays, while for tree-dominated $B \rightarrow PV$ decays, their effects are generally quite small. In

particular, for decay modes dominated by the coefficient $\alpha_4^p(PV)$, these higher order penguin contraction contributions can increase the branching ratios by about 40% \sim 90%, while for those dominated by the coefficient $\alpha_4^p(VP)$, their contributions are also predicted to be small and tend to decrease the branching ratios of these decay modes. At present, all these predicted CP -averaged branching ratios still suffer from large theoretical uncertainties.

3.3 Direct CP -violating asymmetries of $B \rightarrow PV$ decays

In this subsection, we will discuss the direct CP -violating asymmetries. In particular, we will investigate the impact of the higher order penguin contractions of spectator-scattering amplitudes on this quantity.

We adopt the convention for direct CP asymmetries

$$\mathcal{A}_{CP} \equiv \frac{\mathcal{B}(\bar{B}^0 \rightarrow \bar{f}) - \mathcal{B}(B^0 \rightarrow f)}{\mathcal{B}(\bar{B}^0 \rightarrow \bar{f}) + \mathcal{B}(B^0 \rightarrow f)}. \quad (42)$$

Our numerical results for the direct CP -violating asymmetries are listed in Tables 6 and 7. Since the strong phases are suppressed by α_s and/or Λ_{QCD}/m_b within the QCDF formalism, the direct CP -violating asymmetries for most $B \rightarrow PV$ decays are predicted to be typically small. This is particularly true for decay modes dominated by the tree coefficient α_1 , for example, the decay $\bar{B}^0 \rightarrow \pi^- \rho^+$. However, for $b \rightarrow d$ penguin dominated $B \rightarrow K \bar{K}^*$ decays, the penguin amplitudes generated by the internal u-quark loop and c-quark loop are proportional to the comparable CKM elements $V_{ub}^* V_{ud}$ and $V_{cb}^* V_{cd}$, respectively, large direct CP -violating asymmetries for these decay channels are predicted. In addition, due to large interference effects between the tree and penguin amplitudes, the direct CP -violating asymmetry of $B^- \rightarrow \pi^0 K^{*-}$ decay is also predicted to be large.

Due to cancellations among the strong phases associated with the individual Feynman diagram in Fig. 6 as discussed in Sec. 3.1, the higher order penguin contraction contributions to the direct CP -violating asymmetries for most $B \rightarrow PV$ decays are predicted to be small, however with a few exceptions. From Table 6, we can see that both the higher order penguin contraction and the weak annihilation contributions have significant impacts on the direct CP -violating asymmetry of $\bar{B}^0 \rightarrow \pi^0 \rho^0$ decay. This is due to the delicate cancellations among the competing terms in its decay amplitude, making these sub-leading contributing terms potentially large.

Table 6: Direct CP -violating asymmetries (in units of 10^{-2}) for two-body hadronic charmless $B \rightarrow PV$ decays with $\Delta S = 0$. Decay modes with very small branching ratios are not considered. \mathcal{A}_{CP}^f and \mathcal{A}_{CP}^{f+a} denote the results without and with the annihilation contributions, respectively. The other captions are the same as Table 3.

Decay mode	\mathcal{A}_{CP}^f		\mathcal{A}_{CP}^{f+a}		EXP.
	$\mathcal{O}(\alpha_s)$	$\mathcal{O}(\alpha_s + \alpha_s^2)$	$\mathcal{O}(\alpha_s)$	$\mathcal{O}(\alpha_s + \alpha_s^2)$	
$B^- \rightarrow \pi^- \rho^0$	$3.25^{+1.98}_{-1.27}$	$5.26^{+3.62}_{-2.06}$	$3.62^{+2.29}_{-1.43}$	$5.64^{+3.58}_{-2.13}$	-7^{+12}_{-13}
	$2.83^{+2.35}_{-1.33}$	$4.02^{+3.04}_{-1.58}$	$3.39^{+2.36}_{-1.53}$	$4.58^{+2.78}_{-1.78}$	
$B^- \rightarrow \pi^0 \rho^-$	$-2.41^{+0.81}_{-1.61}$	$-3.69^{+1.39}_{-2.48}$	$-2.63^{+0.83}_{-1.63}$	$-3.88^{+1.37}_{-2.52}$	1 ± 11
	$-1.74^{+0.68}_{-1.54}$	$-2.49^{+0.94}_{-1.84}$	$-2.03^{+0.76}_{-1.70}$	$-2.76^{+0.95}_{-1.87}$	
$\bar{B}^0 \rightarrow \pi^+ \rho^-$	$-1.05^{+0.12}_{-0.19}$	$-2.65^{+0.92}_{-1.85}$	$-1.03^{+0.12}_{-0.17}$	$-2.57^{+0.80}_{-1.82}$	-15 ± 9
	$-0.68^{+0.08}_{-0.11}$	$-1.68^{+0.45}_{-1.03}$	$-0.65^{+0.07}_{-0.11}$	$-1.62^{+0.44}_{-0.89}$	
$\bar{B}^0 \rightarrow \pi^- \rho^+$	$0.40^{+0.64}_{-0.37}$	$-0.03^{+0.64}_{-0.60}$	$0.31^{+0.58}_{-0.37}$	$-0.13^{+0.64}_{-0.53}$	-47^{+13}_{-14}
	$-0.76^{+0.23}_{-0.27}$	$-1.36^{+0.41}_{-0.65}$	$-0.88^{+0.23}_{-0.29}$	$-1.49^{+0.40}_{-0.64}$	
$\bar{B}^0 \rightarrow \pi^0 \rho^0$	$-5.64^{+9.80}_{-17.89}$	$5.92^{+10.14}_{-17.18}$	$-13.49^{+11.83}_{-20.61}$	$-0.22^{+12.35}_{-23.54}$	-49^{+70}_{-83}
	$-4.42^{+19.18}_{-28.38}$	$10.58^{+18.83}_{-28.48}$	$-19.13^{+18.98}_{-32.25}$	$-1.68^{+21.36}_{-34.52}$	
$B^- \rightarrow \pi^- \omega$	$-1.95^{+1.54}_{-2.03}$	$-4.49^{+1.68}_{-2.34}$	$-1.84^{+1.58}_{-2.09}$	$-4.45^{+1.66}_{-2.16}$	-4 ± 8
	$-4.46^{+2.11}_{-3.14}$	$-6.66^{+2.38}_{-3.37}$	$-4.36^{+2.10}_{-3.09}$	$-6.64^{+2.42}_{-3.21}$	
$B^- \rightarrow K^- K^{*0}$	$-36.28^{+5.04}_{-5.51}$	$-19.29^{+8.89}_{-6.15}$	$-31.08^{+4.37}_{-4.67}$	$-15.34^{+8.74}_{-6.47}$...
	$-42.06^{+5.68}_{-6.38}$	$-28.33^{+6.84}_{-5.54}$	$-36.92^{+5.40}_{-5.29}$	$-24.27^{+6.78}_{-5.82}$	
$\bar{B}^0 \rightarrow \bar{K}^0 K^{*0}$	$-36.27^{+5.02}_{-5.66}$	$-19.29^{+8.34}_{-6.48}$	$-32.72^{+4.74}_{-4.82}$	$-17.56^{+7.65}_{-5.57}$...
	$-42.06^{+5.43}_{-6.50}$	$-28.33^{+6.91}_{-5.56}$	$-38.64^{+5.15}_{-5.46}$	$-26.25^{+6.10}_{-6.04}$	
$B^- \rightarrow K^0 K^{*-}$	$-12.64^{+4.49}_{-4.14}$	$-22.25^{+4.35}_{-7.40}$	$-9.41^{+5.03}_{-4.82}$	$-15.93^{+4.95}_{-4.54}$...
	$-2.96^{+8.53}_{-6.64}$	$-18.26^{+5.22}_{-9.82}$	$0.18^{+10.23}_{-7.16}$	$-9.17^{+8.89}_{-6.79}$	
$\bar{B}^0 \rightarrow K^0 \bar{K}^{*0}$	$-12.64^{+4.60}_{-4.00}$	$-22.25^{+4.24}_{-8.09}$	$-9.25^{+4.55}_{-4.78}$	$-16.25^{+4.90}_{-4.25}$...
	$-2.96^{+8.64}_{-6.76}$	$-18.26^{+5.59}_{-8.60}$	$-1.76^{+6.45}_{-5.73}$	$-12.22^{+5.90}_{-6.34}$	

From the numerical results given in Tables 6 and 7, we can also see that the higher order penguin contraction contributions to the direct CP -violating asymmetries of $\bar{B}^0 \rightarrow \pi^+ \rho^-$, $B^- \rightarrow \pi^- \omega$,

Table 7: Direct CP -violating asymmetries (in units of 10^{-2}) for two-body hadronic charmless $B \rightarrow PV$ decays with $\Delta S = 1$. The captions are the same as Table 6.

Decay mode	\mathcal{A}_{CP}^f		\mathcal{A}_{CP}^{f+a}		EXP.
	$\mathcal{O}(\alpha_s)$	$\mathcal{O}(\alpha_s + \alpha_s^2)$	$\mathcal{O}(\alpha_s)$	$\mathcal{O}(\alpha_s + \alpha_s^2)$	
$B^- \rightarrow \pi^- \bar{K}^{*0}$	$1.49^{+0.23}_{-0.14}$	$0.76^{+0.26}_{-0.34}$	$1.22^{+0.14}_{-0.13}$	$0.57^{+0.26}_{-0.34}$	-9.3 ± 6.0
	$1.77^{+0.24}_{-0.17}$	$1.14^{+0.21}_{-0.24}$	$1.47^{+0.17}_{-0.15}$	$0.93^{+0.21}_{-0.26}$	
$B^- \rightarrow \pi^0 K^{*-}$	$14.03^{+2.88}_{-2.44}$	$18.21^{+5.43}_{-4.15}$	$11.98^{+2.46}_{-2.10}$	$15.48^{+4.69}_{-3.59}$	4 ± 29
	$13.09^{+3.48}_{-2.66}$	$14.85^{+3.47}_{-3.07}$	$11.27^{+2.74}_{-2.40}$	$12.72^{+2.74}_{-2.43}$	
$\bar{B}^0 \rightarrow \pi^+ K^{*-}$	$9.14^{+1.51}_{-1.34}$	$17.18^{+6.39}_{-4.76}$	$7.11^{+1.31}_{-1.24}$	$13.75^{+5.50}_{-4.06}$	-5 ± 14
	$3.89^{+0.65}_{-0.59}$	$9.16^{+2.87}_{-2.09}$	$2.86^{+0.52}_{-0.49}$	$7.16^{+1.93}_{-1.46}$	
$\bar{B}^0 \rightarrow \pi^0 \bar{K}^{*0}$	$-11.58^{+4.15}_{-8.58}$	$-9.94^{+3.14}_{-4.69}$	$-9.20^{+2.79}_{-5.00}$	$-8.34^{+2.64}_{-3.77}$	-1^{+27}_{-26}
	$-12.14^{+4.04}_{-7.46}$	$-10.06^{+3.09}_{-4.31}$	$-9.97^{+3.36}_{-4.79}$	$-8.60^{+2.47}_{-3.68}$	
$B^- \rightarrow K^- \phi$	$2.08^{+0.53}_{-0.27}$	$1.07^{+0.32}_{-0.37}$	$1.61^{+0.23}_{-0.18}$	$0.78^{+0.30}_{-0.39}$	3.7 ± 5.0
	$2.33^{+0.56}_{-0.31}$	$1.49^{+0.21}_{-0.22}$	$1.84^{+0.27}_{-0.20}$	$1.17^{+0.23}_{-0.23}$	
$\bar{B}^0 \rightarrow \bar{K}^0 \phi$	$2.08^{+0.50}_{-0.27}$	$1.07^{+0.33}_{-0.39}$	$1.72^{+0.27}_{-0.19}$	$0.92^{+0.25}_{-0.39}$	9 ± 14
	$2.33^{+0.58}_{-0.29}$	$1.49^{+0.20}_{-0.23}$	$1.96^{+0.33}_{-0.21}$	$1.30^{+0.19}_{-0.25}$	
$B^- \rightarrow \bar{K}^0 \rho^-$	$0.49^{+0.14}_{-0.17}$	$0.93^{+0.34}_{-0.15}$	$0.37^{+0.17}_{-0.21}$	$0.67^{+0.20}_{-0.18}$...
	$0.11^{+0.25}_{-0.32}$	$0.80^{+0.41}_{-0.20}$	$-0.02^{+0.29}_{-0.40}$	$0.41^{+0.28}_{-0.36}$	
$B^- \rightarrow K^- \rho^0$	$-7.99^{+11.58}_{-5.17}$	$-3.62^{+17.39}_{-6.87}$	$-7.32^{+4.63}_{-3.55}$	$-4.55^{+8.50}_{-4.26}$	31^{+12}_{-11}
	$5.88^{+27.17}_{-10.73}$	$15.31^{+33.85}_{-16.23}$	$-0.38^{+13.62}_{-5.64}$	$5.17^{+23.92}_{-8.71}$	
$\bar{B}^0 \rightarrow K^- \rho^+$	$-1.76^{+1.64}_{-0.87}$	$0.24^{+4.86}_{-1.84}$	$-0.91^{+1.21}_{-0.85}$	$0.46^{+2.99}_{-1.42}$	17^{+15}_{-16}
	$4.12^{+4.76}_{-2.50}$	$7.89^{+10.46}_{-4.88}$	$3.02^{+3.08}_{-1.67}$	$5.44^{+6.24}_{-3.07}$	
$\bar{B}^0 \rightarrow \bar{K}^0 \rho^0$	$9.58^{+3.69}_{-3.24}$	$9.73^{+3.86}_{-3.29}$	$7.65^{+2.85}_{-2.30}$	$7.78^{+2.67}_{-2.45}$...
	$12.36^{+5.78}_{-4.30}$	$12.91^{+5.89}_{-4.81}$	$9.81^{+3.63}_{-3.16}$	$10.23^{+4.29}_{-3.46}$	
$B^- \rightarrow K^- \omega$	$-4.71^{+2.93}_{-2.41}$	$-2.85^{+4.26}_{-3.31}$	$-4.35^{+2.05}_{-1.93}$	$-3.04^{+2.92}_{-2.35}$	2 ± 7
	$4.75^{+13.57}_{-5.57}$	$8.69^{+16.81}_{-7.30}$	$1.39^{+6.29}_{-3.35}$	$3.94^{+9.10}_{-4.60}$	
$\bar{B}^0 \rightarrow \bar{K}^0 \omega$	$-9.65^{+4.10}_{-5.65}$	$-8.90^{+3.91}_{-5.41}$	$-7.61^{+2.96}_{-4.62}$	$-7.13^{+2.69}_{-3.99}$	44 ± 23
	$-12.85^{+5.95}_{-6.22}$	$-11.61^{+5.50}_{-5.40}$	$-10.55^{+4.54}_{-7.83}$	$-9.94^{+4.27}_{-6.60}$	

$\overline{B}^0 \rightarrow \pi^- \rho^+$, and $\overline{B}^0 \rightarrow K^- \rho^+$ decays are also quite large. In particular, these higher order penguin contraction contributions can increase the direct CP -violating asymmetries of the former two, while decrease those of the latter two by the same magnitude.

Although the uncertainties from various input parameters are reduced to some extent, the renormalization scale dependence of the direct CP -violating asymmetries for some decay modes, such as $B^- \rightarrow K^- \omega$ and $B^- \rightarrow K^- \rho^0$ decays, are still large. This is due to the fact that the imaginary parts of the coefficients α_i define by Eq. (10), which are crucial for the direct CP -violating asymmetries, generally have a larger scale dependence [8].

The direct CP -violating asymmetries for some hadronic charmless $B \rightarrow PV$ decays have been measured recently, the data are still too uncertain to draw any meaningful conclusions from the comparison with the theoretical predictions, which also suffer from large uncertainties. With theoretical progresses and the rapid accumulation of experimental data, the situation will be improved and large direct CP -violating asymmetries in some decay channels, for example, the decays $B \rightarrow K \bar{K}^*$, will be found in the near future.

3.4 Detailed analysis of $B \rightarrow \pi K^*$, $K \rho$ decays

The $B \rightarrow \pi K^*$ and $B \rightarrow K \rho$ decays, like their PP counterparts $B \rightarrow \pi K$ decays, are also penguin-dominated decay modes, and hence sensitive to any new physics contributions. If the “ πK ” puzzles, with the improvement of experimental measurements, still remain unexplained within the SM, there would be signals of new physics beyond the SM [27]. Thus, the $B \rightarrow \pi K^*$ and $B \rightarrow K \rho$ decays can be used to determine whether there are any new physics contributions and, which one, if exist as hinted by the “ πK ” puzzles, is more favored. On the other hand, once the data on these decay modes becomes more precise, useful information on the weak phase angle γ can also be obtained from these decay modes [28]. So, detailed studies on these decay modes are worthy.

In Figs. 9 and 10, we show the dependence of the CP -averaged branching ratios of these decay modes on the weak phase γ . In these two and the following figures, the central values of all input parameters except for the CKM angle γ are defaulted and the renormalization scale is fixed at $\mu = m_b$.

From these two figures, we can see that the experimental data on these decay modes are

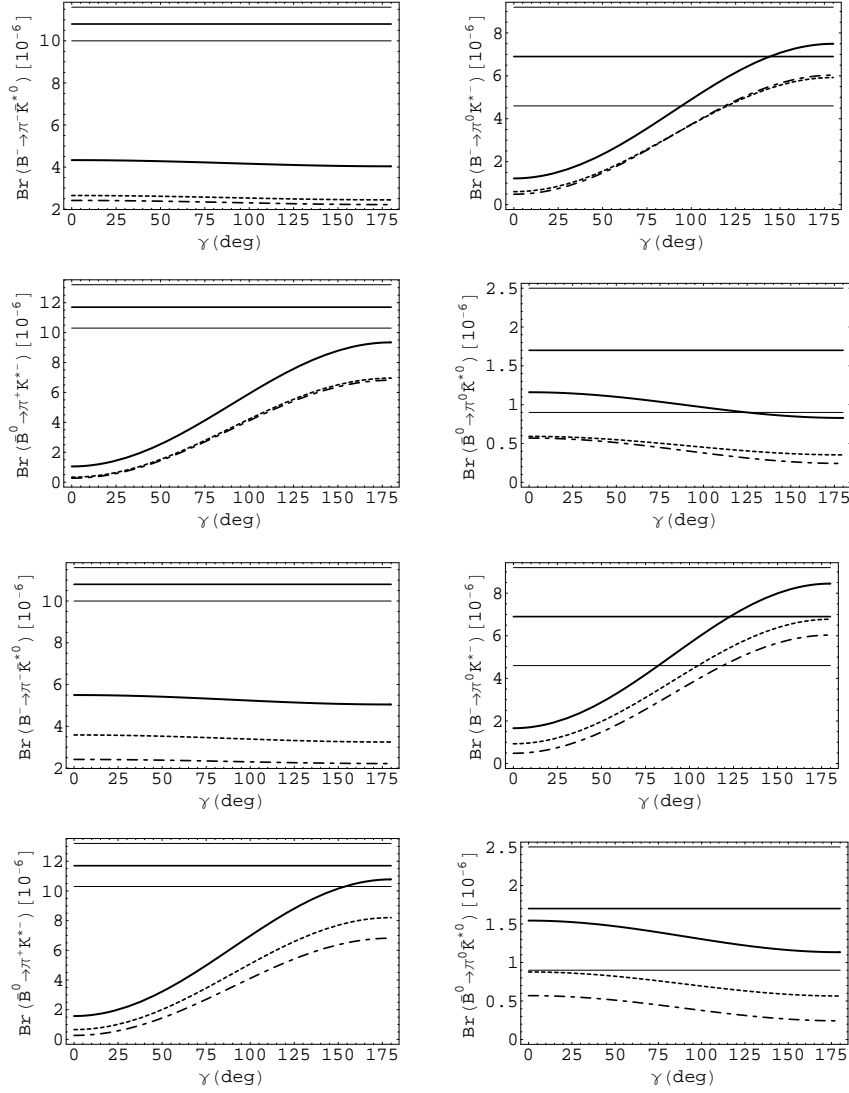


Figure 9: The γ dependence of the CP -averaged branching ratios of $B \rightarrow \pi K^*$ decays. The upper and the lower four plots denote the results without and with the annihilation contributions, respectively. The solid and dashed lines correspond to the theoretical predictions with and without the higher order penguin contraction contributions, respectively. The horizontal solid lines denote the experimental data as given in Table 3, with the thicker ones being its central values and the thinner its error bars. The NF results denoted by the dash-dotted lines are also shown for comparison.

generally larger than the theoretical predictions obtained based on the QCDF approach. Some decay modes, such as $B^- \rightarrow \pi^0 K^{*-}$ and $\bar{B}^0 \rightarrow \pi^+ K^{*-}$ decays, have a strong dependence on the weak angle γ . Moreover, both the higher order penguin contraction and the weak annihilation

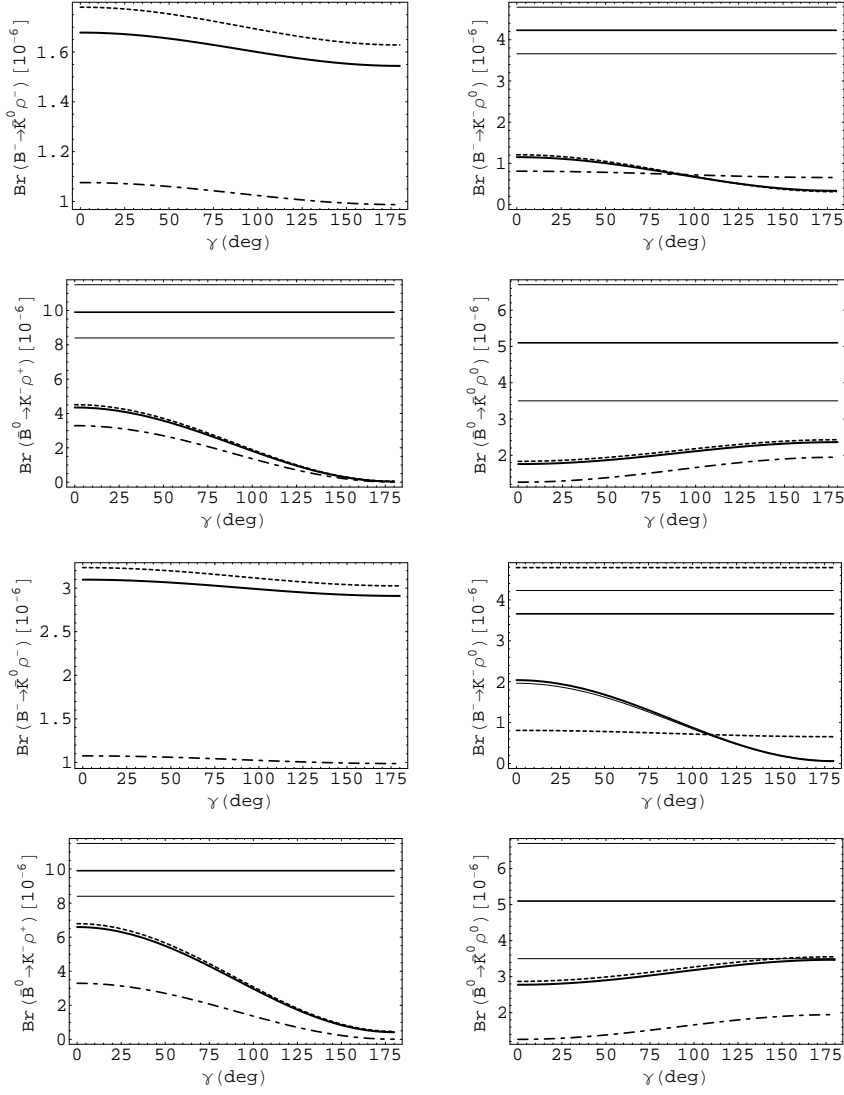


Figure 10: The same as Fig. 9 but for $B \rightarrow K\rho$ decays.

contributions can give significant enhancements to the CP -averaged branching ratios of $B \rightarrow \pi K^*$ decays. However, for $B \rightarrow \pi K^*$ decays, only the weak annihilation contributions can provide large enhancements to the CP -averaged branching ratios, and the higher order penguin contraction contributions play only a minor role.

Since the theoretical uncertainties in the predicted CP -averaged branching ratios can be largely reduced by taking ratios among them, we shall discuss below certain ratios among the CP -averaged branching fractions of these decay modes, like the ones defined for $B \rightarrow \pi K$ decays [29].

For $B \rightarrow \pi K^*$ decays, we define the following three ratios [28]

$$R(\pi K^*) \equiv \frac{\tau_{B_u} \bar{\mathcal{B}}(\bar{B}^0 \rightarrow \pi^+ K^{*-})}{\tau_{B_d} \bar{\mathcal{B}}(B^- \rightarrow \pi^- \bar{K}^{*0})}, \quad (43)$$

$$R_c(\pi K^*) \equiv 2 \frac{\bar{\mathcal{B}}(B^- \rightarrow \pi^0 K^{*-})}{\bar{\mathcal{B}}(B^- \rightarrow \pi^- \bar{K}^{*0})}, \quad (44)$$

$$R_n(\pi K^*) \equiv \frac{1}{2} \frac{\bar{\mathcal{B}}(\bar{B}^0 \rightarrow \pi^+ K^{*-})}{\bar{\mathcal{B}}(\bar{B}^0 \rightarrow \pi^0 \bar{K}^{*0})}. \quad (45)$$

With $\pi(K^*)$ meson replaced by $\rho(K)$ meson, we can get another three similar ratios for $B \rightarrow K\rho$ decays. These ratios should be more appropriate to derive information on the weak phase angle γ , as well as the relative strength of tree and penguin contributions than branching ratios.

Our numerical results and the current experimental data for these ratios are presented in Table 8. The γ dependence of these ratios are displayed in Figs. 11 and 12.

From these two figures and the numerical results given in Table 8, we can see that our theoretical predictions for most of these ratios are in agreement with the data, considering the large uncertainties in the experimental data.

From the explicit expressions of the decay amplitudes for these decay modes as given, for example, in Ref. [12], we can see that differences between the two ratios R_c and R_n for both πK^* and $K\rho$ modes arise mainly from the color-allowed electro-weak penguin coefficient $\alpha_{3,ew}^p$ and the color-suppressed tree coefficient α_2 , which are both predicted to be small within the QCDF formalism. So, the two ratios R_c and R_n are expected to be approximately equal within the SM. However, due to delicate cancellations among various competing terms, these ratios are strongly affected by the sub-leading contributing terms. After including the weak annihilation contributions, the two ratios R_c and R_n tend to be approximately equal. The current experimental data, however, indicate that $R_n(\pi K^*)$ is somewhat larger than $R_c(\pi K^*)$, but with large errors in the former. Unfortunately, due to the insufficient data on the branching ratios of the $K\rho$ modes, direct experimental comparison between $R_c(\rho K)$ and $R_n(\rho K)$ is not feasible for the time being. Once the experimental “ $R_c - R_n$ ” comparison with the case of πK^* and $K\rho$ decays are available, we can determine whether our theoretical predictions based on the QCDF approach are correct.

It is also noted that the patterns of these quantities remain nearly unaffected even with these higher order penguin contributions included, because the higher order penguin contraction

Table 8: Ratios among the CP -averaged branching fractions of $B \rightarrow \pi K^*, K\rho$ decays. Numbers shown in columns 3 and 4 correspond to the results obtained without the annihilation contributions, while those in columns 5 and 6 the ones with the annihilation contributions. The other captions are the same as in Table 3.

	NF	$\mathcal{O}(\alpha_s)$	$\mathcal{O}(\alpha_s + \alpha_s^2)$	$\mathcal{O}(\alpha_s)$	$\mathcal{O}(\alpha_s + \alpha_s^2)$	EXP.
$R(\pi K^*)$	$0.84^{+0.16}_{-0.14}$	$0.80^{+0.18}_{-0.14}$	$0.77^{+0.14}_{-0.11}$	$0.76^{+0.15}_{-0.12}$	$0.76^{+0.12}_{-0.11}$	1.18 ± 0.17
	$0.75^{+0.11}_{-0.09}$	$0.74^{+0.16}_{-0.11}$	$0.74^{+0.11}_{-0.11}$	$0.72^{+0.15}_{-0.10}$	$0.73^{+0.11}_{-0.10}$	
$R_c(\pi K^*)$	$1.53^{+0.45}_{-0.31}$	$1.45^{+0.49}_{-0.31}$	$1.28^{+0.29}_{-0.22}$	$1.33^{+0.37}_{-0.26}$	$1.22^{+0.25}_{-0.20}$	1.28 ± 0.44
	$1.24^{+0.27}_{-0.21}$	$1.32^{+0.45}_{-0.27}$	$1.22^{+0.28}_{-0.20}$	$1.24^{+0.32}_{-0.23}$	$1.17^{+0.23}_{-0.19}$	
$R_n(\pi K^*)$	$1.87^{+0.94}_{-0.53}$	$1.80^{+1.14}_{-0.53}$	$1.41^{+0.51}_{-0.32}$	$1.54^{+0.66}_{-0.42}$	$1.31^{+0.42}_{-0.26}$	3.44 ± 1.68
	$1.37^{+0.48}_{-0.29}$	$1.58^{+0.80}_{-0.44}$	$1.33^{+0.50}_{-0.28}$	$1.40^{+0.53}_{-0.34}$	$1.25^{+0.43}_{-0.24}$	
$R(\rho K)$	$2.55^{+2.45}_{-0.94}$	$2.12^{+1.54}_{-0.67}$	$2.17^{+1.73}_{-0.72}$	$1.78^{+0.85}_{-0.41}$	$1.80^{+0.87}_{-0.41}$	> 0.22
	$3.20^{+6.80}_{-1.48}$	$2.41^{+2.62}_{-0.85}$	$2.53^{+2.78}_{-0.93}$	$1.91^{+1.04}_{-0.50}$	$1.97^{+1.16}_{-0.55}$	
$R_c(\rho K)$	$1.47^{+1.96}_{-0.66}$	$1.14^{+0.99}_{-0.41}$	$1.16^{+1.12}_{-0.43}$	$0.98^{+0.53}_{-0.26}$	$0.99^{+0.56}_{-0.30}$	> 0.18
	$1.52^{+4.78}_{-0.80}$	$1.14^{+1.49}_{-0.49}$	$1.21^{+1.76}_{-0.55}$	$0.94^{+0.60}_{-0.31}$	$0.95^{+0.75}_{-0.29}$	
$R_n(\rho K)$	$0.88^{+0.44}_{-0.26}$	$0.87^{+0.34}_{-0.23}$	$0.87^{+0.35}_{-0.24}$	$0.87^{+0.25}_{-0.20}$	$0.87^{+0.26}_{-0.21}$	0.97 ± 0.34
	$0.87^{+0.52}_{-0.26}$	$0.84^{+0.39}_{-0.23}$	$0.85^{+0.40}_{-0.27}$	$0.84^{+0.26}_{-0.20}$	$0.84^{+0.26}_{-0.21}$	

contributions to the decays in the same ratio are similar in nature, and hence eliminated.

With refined measurements available in the forthcoming years, it would be very interesting to check whether the theoretical predictions for these ratios are consistent with the data. Moreover, studies on these $B \rightarrow PV$ modes will help us to understand the “ πK ” puzzles [27].

4 Conclusions

In this paper, we have reexamined the hadronic charmless $B \rightarrow PV$ (with $P = (\pi, K)$, and $V = (\rho, K^*, \omega, \phi)$) decays in the framework of the QCDF. We have taken into account the penguin contractions of spectator-scattering amplitudes induced by the $b \rightarrow Dg^*g^*$ transitions, which are of order α_s^2 . The main conclusions of this paper are summarized as follows.

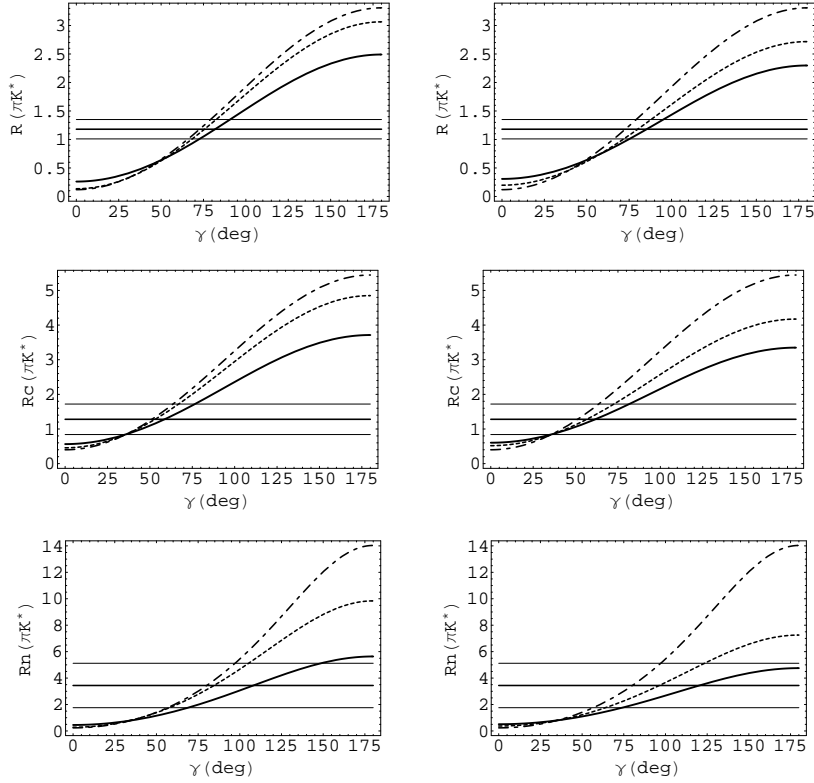


Figure 11: Ratios of the CP -averaged branching fractions for $B \rightarrow \pi K^*$ decays defined by Eqs. (43)–(45) as functions of the weak phase γ . The left and the right plots denote the results without and with the annihilation contributions, respectively. The meaning of the other lines is the same as in Fig. 9.

1. For penguin-dominated $B \rightarrow PV$ decays, predictions obtained based on the QCDF approach are generally quite different from the ones obtained with the NF approximation due to large “nonfactorizable” effects on the penguin coefficients. Contrary to their PP counterparts, the PV modes usually have smaller penguin coefficients α_4^p , rendering the sub-dominant terms potentially large. For example, the weak annihilation contributions, though power suppressed by Λ_{QCD}/m_b , are very significant in these penguin-dominated decays. The higher order penguin contraction contributions can interfere significantly with the next-to-leading order results, and hence are also important for these penguin-dominated decay modes. In particular, for decay modes dominated by the coefficient $\alpha_4^p(PV)$, the higher order penguin contraction contributions can increase the CP -averaged branching ratios by about 40% \sim 90%, while for those dominated by the coefficient

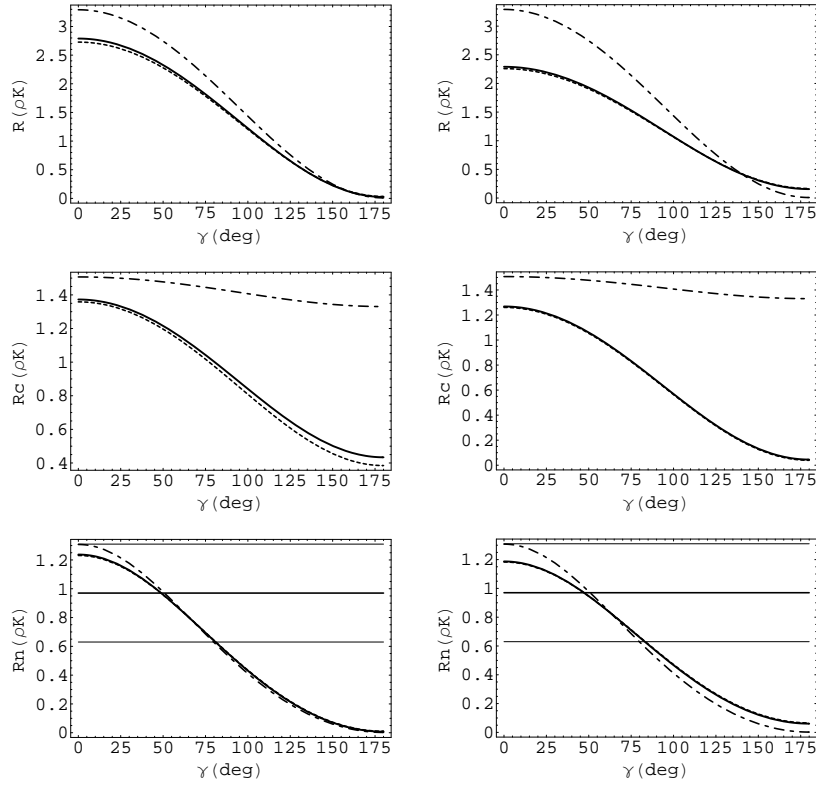


Figure 12: The same as Fig. 11 but for $B \rightarrow K\rho$ decays

$\alpha_4^p(VP)$, their contributions are predicted to be small and tend to decrease the branching ratios of these decay modes.

2. For tree-dominated decays and the decays having only the penguin coefficients α_3^p , $\alpha_{3,ew}^p$ or having only the weak annihilation contributions, the higher order penguin contraction contributions to the CP -averaged branching ratios are predicted to be quite small.
3. Since the direct CP -violating asymmetries are proportional to the sin of strong phase, which is usually suppressed by α_s and/or Λ_{QCD}/m_b within the QCDF formalism, most of the hadronic charmless $B \rightarrow PV$ decays are predicted to have typically small direct CP -violating asymmetries. However, for those decay modes where there are large interference effects between various contributing terms in the decay amplitudes, such as $B \rightarrow KK^*$ decays, large direct CP -violating asymmetries are predicted.
4. Due to large cancellations among the strong phases associated with the individual Feyn-

man diagram in Fig. 6, the higher order penguin contraction contributions to the direct CP -violating asymmetries for most $B \rightarrow PV$ decays are predicted to be small, however with a few exceptions. For example, we find that both the higher order penguin contraction and the weak annihilation contributions have significant impacts on the direct CP -violating asymmetry of $\bar{B}^0 \rightarrow \pi^0 \rho^0$ decay. In addition, the higher order penguin contraction contributions to the direct CP -violating asymmetries of $\bar{B}^0 \rightarrow \pi^+ \rho^-$, $B^- \rightarrow \pi^- \omega$, $\bar{B}^0 \rightarrow \pi^- \rho^+$, and $\bar{B}^0 \rightarrow K^- \rho^+$ decays are also quite large.

5. With more accurate experimental measurements available in the forthcoming years, it would be very interesting to check whether the theoretical predictions for the ratios R , R_c , and R_n for both the πK^* and $K \rho$ decay modes are consistent with the experimental data. In particular, the experimental $R_c - R_n$ comparison with the case of πK^* and ρK decays are very crucial for our understandings of the “ πK ” puzzles.

Although the theoretical results presented here still have large uncertainties, the penguin contractions of spectator-scattering amplitudes induced by the $b \rightarrow Dg^*g^*$ transitions, which are of order α_s^2 , have been shown to be very important for two-body hadronic charmless $B \rightarrow PV$ decays, particularly for those penguin-dominated ones. It is very interesting to note that the 1-loop (α_s^2) correction to the hard spectator scattering in the tree-dominated $B \rightarrow \pi\pi$ decays has been performed recently [30], which forms another part of the NNLO contribution to the QCD factorization formula for hadronic B -meson decays. Using the PQCD method, the NLO corrections have also been carried out for $B \rightarrow \pi\pi, \pi K$ and $\rho\rho$ decays very recently [31]. In addition, much progresses in SCET have also been made in the past two years [32]. With the steady progress in experimental measurements at BaBar and Belle, further systematic studies on these higher order contributions to the rare hadronic B -meson decays are therefore interesting and deserving.

Acknowledgments

We thank Prof. Y. B. Dai for helpful discussions. The work is supported by National Science Foundation under contract No. 10305003, Henan Provincial Foundation for Prominent Young Scientists under contract No. 0312001700, and the NCET Program sponsored by Ministry of

APPENDIX A: ANALYTIC EXPRESSIONS FOR THE Δ_i FUNCTIONS

In the NDR scheme, after performing the loop momentum integration, subtracting the regulator ϵ using the $\overline{\text{MS}}$ scheme, and performing the Feynman parameter integrals, we get the analytic expressions for the Δ_i functions appearing in Eqs. (36) and (37)

$$\Delta i_5 = 2 + \frac{2r_1}{r_3} [G_0(r_1) - G_0(r_1 + r_3)] - \frac{4}{r_3} [G_{-1}(r_1) - G_{-1}(r_1 + r_3)], \quad (46)$$

$$\begin{aligned} \Delta i_6 = & -2 - \frac{4}{r_3} + \frac{2r_1(1+r_3)}{r_3^2} G_0(r_1) - \frac{2(r_1+r_3+r_1r_3)}{r_3^2} G_0(r_1+r_3) \\ & + \frac{4}{r_3} [G_{-1}(r_1) - G_{-1}(r_1+r_3)] - \frac{(4-r_1)r_1}{r_3^2} T_0(r_1) \\ & + \frac{(4-r_1-r_3)(r_1+r_3)}{r_3^2} T_0(r_1+r_3), \end{aligned} \quad (47)$$

$$\Delta i_{23} = -2 - \frac{2r_1}{r_3} [G_0(r_1) - G_0(r_1 + r_3)] + \frac{4}{r_3} [G_{-1}(r_1) - G_{-1}(r_1 + r_3)], \quad (48)$$

$$\Delta i_{26} = -\Delta i_{23}, \quad (49)$$

$$\begin{aligned} \Delta i_2 = & -\frac{22}{9} + \frac{8}{3} \ln \frac{\mu}{m_c} - \frac{2(8+r_1)}{3r_3} G_0(r_1) + \frac{2(8+r_1-2r_3)}{3r_3} G_0(r_1+r_3) \\ & + \frac{4}{r_3} [G_{-1}(r_1) - G_{-1}(r_1+r_3)], \end{aligned} \quad (50)$$

$$\begin{aligned} \Delta i_3 = & \frac{22}{9} + \frac{12}{r_3} + \frac{4r_1}{3r_3} - \frac{8}{3} \ln \frac{\mu}{m_c} - \frac{2(7r_1-r_3-3r_1r_3+2r_1^2-2r_3^2)}{3r_3^2} G_0(r_1+r_3) \\ & + \frac{2r_1(7+2r_1-3r_3)}{3r_3^2} G_0(r_1) - \frac{4(2r_1+r_3)}{r_3^2} [G_{-1}(r_1) - G_{-1}(r_1+r_3)] \\ & + \frac{3(4-r_1)r_1}{r_3^2} T_0(r_1) - \frac{3(4-r_1-r_3)(r_1+r_3)}{r_3^2} T_0(r_1+r_3), \end{aligned} \quad (51)$$

$$\Delta i_8 = \frac{32}{9} - \frac{16}{3} \ln \frac{\mu}{m_c} - \frac{8(2+r_1)}{3r_3} G_0(r_1) + \frac{8(2+r_1+r_3)}{3r_3} G_0(r_1+r_3), \quad (52)$$

$$\begin{aligned} \Delta i_{12} = & -\frac{32}{9} + \frac{12}{r_3} + \frac{4r_1}{3r_3} + \frac{16}{3} \ln \frac{\mu}{m_c} + \frac{2r_1(7+2r_1+6r_3)}{3r_3^2} G_0(r_1) \\ & - \frac{2(2r_1^2-r_3(1-4r_3)+r_1(7+6r_3))}{3r_3^2} G_0(r_1+r_3) \\ & - \frac{8r_1}{r_3^2} [G_{-1}(r_1) - G_{-1}(r_1+r_3)] + \frac{3(4-r_1)r_1}{r_3^2} T_0(r_1) \end{aligned}$$

$$-\frac{3(4-r_1-r_3)(r_1+r_3)}{r_3^2} T_0(r_1+r_3) \quad (53)$$

$$\begin{aligned} \Delta i_{17} = & \frac{2}{3} + \frac{2(8+r_1)}{3r_3} G_0(r_1) - \frac{2}{3} \left(\frac{8+r_1}{r_3} + \frac{4}{r_1+r_3} \right) G_0(r_1+r_3) \\ & - \frac{4}{r_3} [G_{-1}(r_1) - G_{-1}(r_1+r_3)], \end{aligned} \quad (54)$$

$$\begin{aligned} \Delta i_{21} = & -\frac{2}{3} - \frac{16}{r_3} - \frac{8r_1}{3r_3} + \frac{2r_1(4r_1^2+3r_3(8+r_3)+r_1(20+7r_3))}{3r_3^2(r_1+r_3)} G_0(r_1+r_3) \\ & - \frac{2r_1(20+4r_1+3r_3)}{3r_3^2} G_0(r_1) + \frac{4(4r_1+r_3)}{r_3^2} [G_{-1}(r_1) - G_{-1}(r_1+r_3)] \\ & - \frac{4(4-r_1)r_1}{r_3^2} T_0(r_1) + \frac{4(4-r_1-r_3)(r_1+r_3)}{r_3^2} T_0(r_1+r_3), \end{aligned} \quad (55)$$

where the notations $r_1 = k^2/m_c^2$, $r_2 = p^2/m_c^2$, and $r_3 = 2(k \cdot p)/m_c^2$ have been introduced. With m_c replaced by m_b , we can get the results for the b-quark loops. For light u, d, s quark propagating in the fermion loops, these Δi functions can be evaluated straightforwardly. Here only the relevant Δi functions are given. Explicit expressions for the remaining ones can be obtained similarly.

The functions $G_i(t)$ and $T_i(t)$ are defined, respectively, by

$$G_i(t) = \int_0^1 dx x^i \ln[1 - x(1-x)t - i\delta], \quad (56)$$

$$T_i(t) = \int_0^1 dx \frac{x^i}{1 - x(1-x)t - i\delta}, \quad (57)$$

with the explicit form for $T_0(t)$ given by [19]

$$T_0(t) = \begin{cases} \frac{4 \arctan \sqrt{\frac{t}{4-t}}}{\sqrt{t(4-t)}}, & 0 \leq t \leq 4 \\ \frac{2i\pi + 2 \ln(\sqrt{t} - \sqrt{t-4}) - 2 \ln(\sqrt{t} + \sqrt{t-4})}{\sqrt{t(t-4)}}, & t > 4. \end{cases}, \quad (58)$$

while the explicit form for $G_{-1,0}(t)$ could be found in Ref. [17].

APPENDIX B: INPUT PARAMETERS

In this appendix, we present the relevant input parameters used in our numerical calculations as follows.

Wilson coefficients.—The Wilson coefficients $C_i(\mu)$ have been reliably evaluated to next-to-leading logarithmic order [23, 33]. Their numerical values in the NDR scheme at the scale

$\mu = m_b$ ($\mu_h = \sqrt{\Lambda_h m_b}$) are given by

$$\begin{aligned}
C_1 &= 1.080 \ (1.185), \quad C_2 = -0.180 \ (-0.367), \quad C_3 = 0.014 \ (0.028), \\
C_4 &= -0.035 \ (-0.062), \quad C_5 = 0.009 \ (0.011), \quad C_6 = -0.040 \ (-0.085), \\
C_7/\alpha_{\text{e.m.}} &= -0.009 \ (-0.029), \quad C_8/\alpha_{\text{e.m.}} = 0.050 \ (0.107), \quad C_9/\alpha_{\text{e.m.}} = -1.238 \ (-1.375), \\
C_{10}/\alpha_{\text{e.m.}} &= 0.243 \ (0.451), \quad C_{7\gamma}^{\text{eff}} = -0.302 \ (-0.365), \quad C_{8g}^{\text{eff}} = -0.145 \ (-0.169), \quad (59)
\end{aligned}$$

with the input parameters fixed as [34]: $\alpha_s(m_Z) = 0.1187$, $\alpha_{\text{e.m.}}(m_W) = 1/129$, $m_W = 80.425$ GeV, $m_Z = 91.188$ GeV, $\sin^2 \theta_W = 0.2312$, $m_t = 172.7$ GeV [35], $m_b = 4.65$ GeV, $\Lambda_h = 0.5$ GeV.

The CKM matrix elements.—Here we use the Wolfenstein parametrization for the CKM matrix elements [36]

$$V_{\text{CKM}} = \begin{pmatrix} 1 - \frac{\lambda^2}{2} & \lambda & A\lambda^3(\rho - i\eta) \\ -\lambda & 1 - \frac{\lambda^2}{2} & A\lambda^2 \\ A\lambda^3(1 - \rho - i\eta) & -A\lambda^2 & 1 \end{pmatrix} + \mathcal{O}(\lambda^4), \quad (60)$$

and choose the four Wolfenstein parameters (A , λ , ρ , and η) as [37]

$$A = 0.825_{-0.019}^{+0.011}, \quad \lambda = 0.22622 \pm 0.00100, \quad \bar{\rho} = 0.207_{-0.043}^{+0.036}, \quad \bar{\eta} = 0.340 \pm 0.023, \quad (61)$$

with $\bar{\rho}$ and $\bar{\eta}$ defined by $\bar{\rho} = \rho(1 - \frac{\lambda^2}{2})$, $\bar{\eta} = \eta(1 - \frac{\lambda^2}{2})$.

Masses and lifetimes.—For the quark mass, there are two different classes appearing in the QCDF approach. One type is the pole quark mass which appears in the evaluation of the penguin loop corrections, and is denoted by m_q . In this paper, we take

$$m_u = m_d = m_s = 0, \quad m_c = 1.46 \text{ GeV}, \quad m_b = 4.65 \text{ GeV}. \quad (62)$$

The other one is the current quark mass which appears through the equations of motion and in the factor r_χ^M . This kind of quark mass is scale dependent. Following Ref. [12], we hold $(\bar{m}_u + \bar{m}_d)(\mu)/\bar{m}_s(\mu)$ fixed, and use $\bar{m}_s(\mu)$ as an input parameter with the following values

$$\begin{aligned}
2\bar{m}_s(\mu)/(\bar{m}_u + \bar{m}_d)(\mu) &= 24.2, \quad \bar{m}_s(2 \text{ GeV}) = (98 \pm 20) \text{ MeV} [38], \\
\bar{m}_b(\bar{m}_b) &= 4.26 \text{ GeV} [34], \quad (63)
\end{aligned}$$

where the difference between the u and d quark is not distinguished.

For the lifetimes and the masses of the B mesons, we choose

$$\begin{aligned}\tau_{B_u} &= 1.643 \text{ ps [26]}, & m_{B_u} &= 5279.0 \text{ MeV [34]}, \\ \tau_{B_d} &= 1.527 \text{ ps [26]}, & m_{B_d} &= 5279.4 \text{ MeV [34]},\end{aligned}\tag{64}$$

as our default input values. The masses of the light mesons are also chosen from Ref. [34].

Light-cone distribution amplitudes (LCDAs) of mesons.—The LCDAs of mesons are also basic input parameters in this approach. In the heavy quark limit, the light-cone projectors for the B , the pseudoscalar, and the vector mesons in the momentum space can be expressed, respectively, as [3, 12]

$$\mathcal{M}_{\alpha\beta}^B = -\frac{if_B m_B}{4} \left[(1 + \not{v}) \gamma_5 \left\{ \Phi_1^B(\xi) + \not{v}_- \Phi_2^B(\xi) \right\} \right]_{\alpha\beta},\tag{65}$$

$$M_{\alpha\beta}^P = \frac{if_P}{4} \left[\not{p} \gamma_5 \Phi_P(x) - \mu_P \gamma_5 \frac{k_2^\perp k_1^\perp}{k_1 \cdot k_2} \Phi_p(x) \right]_{\alpha\beta},\tag{66}$$

$$(M_{\parallel}^V)_{\alpha\beta} = -\frac{if_V}{4} \left[\not{p} \Phi_V(x) - \frac{m_V f_V^\perp}{f_V} \frac{k_2^\perp k_1^\perp}{k_1 \cdot k_2} \Phi_v(x) \right]_{\alpha\beta},\tag{67}$$

where k_1 and k_2 are the quark and anti-quark momenta of the meson constituents and defined, respectively, by

$$k_1^\mu = xp^\mu + k_\perp^\mu + \frac{\vec{k}_\perp^2}{2xp \cdot \bar{p}} \bar{p}^\mu, \quad k_2^\mu = (1-x)p^\mu - k_\perp^\mu + \frac{\vec{k}_\perp^2}{2(1-x)p \cdot \bar{p}} \bar{p}^\mu.\tag{68}$$

It is understood that only after the factor $k_1 \cdot k_2$ in the denominator of Eqs. (66) and (67) cancelled, can we take the collinear approximation, i.e., the momentum k_1 and k_2 can be set to be xp and $(1-x)p$, respectively, with p being the momentum of the meson. $\Phi_M(x)$ and $\Phi_m(x)$ are the leading twist and twist-3 LCDAs of the meson M , respectively. Since the QCDF approach is based on the heavy quark assumption, to a very good approximation, we can use the asymptotic forms of the LCDAs [39, 40]³

$$\Phi_P(x) = \Phi_V(x) = 6x(1-x), \quad \Phi_p(x) = 1, \quad \Phi_v(x) = 3(2x-1).\tag{69}$$

³It should be noted [12, 39] that, in defining the light-cone projectors of light mesons, all three-particle contributions have been neglected. The leading-twist LCDAs are conventionally expanded in Gegenbauer polynomials

$$\Phi_M(x, \mu) = 6x(1-x) \left[1 + \sum_{n=1}^{\infty} \alpha_n^M(\mu) C_n^{(3/2)}(2x-1) \right],$$

where the Gegenbauer moments $\alpha_n^M(\mu)$ are multiplicatively renormalized. The asymptotic form of the leading twist distribution amplitude is valid in the limit $\mu \rightarrow \infty$. With three-particle contributions being neglected, the twist-3 two-particle distribution amplitudes are then determined completely by the equations of motion.

With respect to the endpoint divergence associated with the momentum fraction integral over the meson LCDAs, following the treatment in Refs. [8, 24], we regulate the integral with an *ad-hoc* cut-off

$$\int_0^1 \frac{dx}{x} \rightarrow \int_{\Lambda_h/m_B}^1 \frac{dx}{x} = \ln \frac{m_B}{\Lambda_h}, \quad (70)$$

with $\Lambda_h = 0.5 \text{ GeV}$. The possible complex phase associated with this integral has been neglected.

As for the B meson wave functions, we need only consider the first inverse moment of the LCDA $\Phi_1^B(\xi)$ defined by [8]

$$\int_0^1 \frac{d\xi}{\xi} \Phi_1^B(\xi) \equiv \frac{m_B}{\lambda_B}, \quad (71)$$

where the hadronic parameter λ_B has been introduced to parameterize this integral. In this paper, we take $\lambda_B = (460 \pm 110) \text{ MeV}$ as our input value [41].

Decay constants and transition form factors.— The decay constants and the form factors are nonperturbative parameters and can be determined from experiments and/or theoretical estimations, such as lattice calculations, QCD sum rules, etc. For their definitions, we refer the readers to Refs. [1, 39, 40]. In this paper, we take the following numerical values for these input parameters

$$\begin{aligned} f_\pi &= 130.7 \text{ MeV} [34], & f_K &= 159.8 \text{ MeV} [34], & f_B &= 216 \text{ MeV} [42], \\ f_\rho &= 205 \text{ MeV} [43], & f_\omega &= 195 \text{ MeV} [43], & f_{K^*} &= 217 \text{ MeV} [43], \\ f_\phi &= 231 \text{ MeV} [43], & f_\rho^\perp(1 \text{ GeV}) &= 160 \text{ MeV} [43], & f_\omega^\perp(1 \text{ GeV}) &= 145 \text{ MeV} [43], \\ f_{K^*}^\perp(1 \text{ GeV}) &= 185 \text{ MeV} [43], & f_\phi^\perp(1 \text{ GeV}) &= 200 \text{ MeV} [43], \\ F_+^{B \rightarrow \pi}(0) &= (0.258 \pm 0.031) [43], & F_+^{B \rightarrow K}(0) &= (0.331 \pm 0.041) [43], \\ A_0^{B \rightarrow \rho}(0) &= (0.303 \pm 0.028) [43], & A_0^{B \rightarrow K^*}(0) &= (0.374 \pm 0.034) [43], \\ A_0^{B \rightarrow \omega}(0) &= (0.281 \pm 0.030) [43], \end{aligned} \quad (72)$$

where the form factors are evaluated at the maximal recoil region. The dependence of the form factors on the momentum-transfer q^2 can be found in Ref. [43]. It should be noted that the transverse decay constant f_V^\perp is scale dependent.

APPENDIX C: THE GAUGE INDEPENDENCE

In this appendix, we present a detail checking of gauge independence of our calculation.

Firstly, we would check the gauge dependence of Fig.5(b) with the gluon propagator

$$D^{\mu\nu}(q^2) = \frac{1}{q^2} \left(g^{\mu\nu} - \xi \frac{q^\mu q^\nu}{q^2} \right), \quad (73)$$

where the factor $-i\delta^{ab}$ has been suppressed, and ξ is the gauge dependent parameter.

Before the light-cone projectors for mesons are sandwiched, the scattering amplitude of this diagram is read as

$$\mathcal{A} \propto \left[\bar{v}_d(p_1) \gamma_\alpha v_d(p_2) \right] \left[\bar{u}_u(p_3) \gamma_\nu \frac{i}{\not{V}} \gamma_\beta v_u(p_4) \right] \left[\bar{u}_s(p_5) \sigma_{\mu\rho} q^\rho (1 + \gamma_5) u_b(p_b) \right] D^{\alpha\beta}(k^2) D^{\mu\nu}(q^2), \quad (74)$$

where the spin indices, color indices, and $SU(3)$ color matrices have been suppressed. It is easy to show that

$$\begin{aligned} \left[\bar{v}_d(p_1) \gamma_\alpha v_d(p_2) \right] D^{\alpha\beta}(k^2) &= \frac{1}{(p_2 - p_1)^2} \left\{ \left[\bar{v}_d(p_1) \gamma^\beta v_d(p_2) \right] \right. \\ &\quad \left. - \xi \left[\bar{v}_d(p_1) (\not{p}_2 - \not{p}_1) v_d(p_2) \right] \frac{p_2^\beta - p_1^\beta}{(p_2 - p_1)^2} \right\} \\ &= \left[\bar{v}_d(p_1) \gamma^\beta v_d(p_2) \right] \frac{1}{(p_2 - p_1)^2}, \end{aligned} \quad (75)$$

where $k = p_2 - p_1$ is the momentum of the gluon connected to the spectator \bar{d} quark, p_1 and p_2 are the momentum of \bar{d} quark before and after scattering, respectively. In the last step, we have used the on-shell condition $\bar{v}_d(p_1)(\not{p}_1 + m_d) = (\not{p}_2 + m_d)v_d(p_2) = 0$. It is also easy to show that

$$\begin{aligned} \left[\bar{u}_s(p_5) \sigma_{\mu\rho} q^\rho (1 + \gamma_5) u_b(p_b) \right] D^{\mu\nu}(q^2) &= \frac{1}{q^2} \left\{ \left[\bar{u}_s(p_5) \sigma^{\nu\rho} q_\rho (1 + \gamma_5) u_b(p_b) \right] \right. \\ &\quad \left. - \xi \frac{q^\nu}{q^2} \left[\bar{u}_s(p_5) \sigma^{\mu\rho} q_\mu q_\rho (1 + \gamma_5) u_b(p_b) \right] \right\} \\ &= \frac{1}{q^2} \left[\bar{u}_s(p_5) \sigma^{\nu\rho} q_\rho (1 + \gamma_5) u_b(p_b) \right]. \end{aligned} \quad (76)$$

From Eq. (76), we can see that the gauge invariance of Q_{8g} removes the gauge-dependent ξ term.

From Eqs. (74), (75), and (76), we can see that the scattering amplitude of Fig.5(b) is independent of the gauge parameter ξ . The above proof could be directly extended to that of

Fig.5(c), Fig.6(b) and (c), since the building blocks $I_\mu^a(k)$ and $\tilde{I}_\mu^a(k)$ defined by Eq.17 are also gauge-invariant, i.e., $k^\mu I_\mu^a(k) = k^\mu \tilde{I}_\mu^a(k) = 0$.

For Fig.5(a), its amplitude reads

$$\begin{aligned} \mathcal{A} \propto & \left[\bar{v}_d(p_1) \gamma_\alpha v_d(p_2) \right] \left[\bar{u}_u(p_3) \gamma_\nu v_u(p_4) \right] \left[\bar{u}_s(p_5) \sigma_{\mu\rho} q^\rho (1 + \gamma_5) u_b(p_b) \right] \\ & \times D^{\alpha\alpha'}(k^2) D^{\nu\nu'}(p^2) D^{\mu\mu'}(q^2) V_{\mu'\nu'\alpha'}(q, p, k), \end{aligned} \quad (77)$$

where $V_{\mu'\nu'\alpha'}(q, p, k)$ is the triple-gluon vertex. One can observe that the amplitude is gauge independent, because of

$$\xi k^\alpha \left[\bar{v}_d(p_1) \gamma_\alpha v_d(p_2) \right] = 0, \quad (k = p_2 - p_1), \quad (78)$$

$$\xi p^\nu \left[\bar{u}_u(p_3) \gamma_\nu v_u(p_4) \right] = 0, \quad (p = p_3 + p_4), \quad (79)$$

$$\xi q^\mu \left[\bar{u}_s(p_5) \sigma_{\mu\rho} q^\rho (1 + \gamma_5) u_b(p_b) \right] = 0. \quad (80)$$

Similarly, we can find that the amplitude of Fig.6(a) is also gauge independent. Using Eqs. (78) and (79), one can find that the amplitudes of Fig.6(d) and (e) are gauge independent.

In summary, we have shown that the amplitudes of the Feynman diagrams in Figs.5 and 6 are gauge independent. The gauge independence of this subset Feynman diagrams is guaranteed by the on-shell external quarks and the gauge-invariance of \mathcal{O}_{8g} and 4-quarks operation insertions $I_\mu^a(k)$ and $\tilde{I}_\mu^a(k)$. There are many $\mathcal{O}(\alpha_s^2)$ Feynman diagrams belonging to the group in Fig.4 but not shown there. For example, the processes $b \rightarrow sg^*$ followed by $g^* \rightarrow \bar{q}_i q_i \rightarrow g^* \rightarrow \bar{u}u$ or a gluon loop, which are gauge dependent separately. To keep gauge-independent, one must calculate the full set of Feynman diagrams in the category of Fig.4, which are not calculated in this paper.

References

- [1] M. Bauer, B. Stech, and M. Wirbel, Z. Phys. C **29**, 637 (1985); **34**, 103 (1987).
- [2] T. W. Yeh and H-n. Li, Phys. Rev. D **56**, 1615 (1997). Y. Y. Keum, H-n. Li, and A. I. Sanda, Phys. Lett. B **504**, 6 (2001); Phys. Rev. D **63**, 054008 (2001).
- [3] M. Beneke, G. Buchalla, M. Neubert, C. T. Sachrajda, Phys. Rev. Lett. **83**, 1914 (1999); Nucl. Phys. B **591**, 313 (2000).

- [4] C. W. Bauer, D. Pirjol, and I. W. Stewart, Phys. Rev. Lett. **87**, 201806 (2001); Phys. Rev. D **65**, 054022 (2002); **67**, 071502 (2003); J. Chay and C. Kim, Phys. Rev. D **65**, 114016 (2002); M. Beneke, A. P. Chapovsky, M. Diehl, and T. Feldmann, Nucl. Phys. B **643**, 431 (2002).
- [5] Y. L. Wu and Y. F. Zhou, Phys. Rev. D **72**, 034037 (2005); C. W. Chiang, M. Gronau, J. L. Rosner, and D. A. Suprun, Phys. Rev. D **70**, 034020 (2004).
- [6] C. W. Chiang, M. Gronau, Z. Luo, J. L. Rosner, and D. A. Suprun, Phys. Rev. D **69**, 034001 (2004).
- [7] Y. Y. Keum and H. n. Li, Phys. Rev. D **63**, 074006 (2001).
- [8] M. Beneke, G. Buchalla, M. Neubert and C. T. Sachrajda, Nucl. Phys. B **606**, 245 (2001).
- [9] T. Muta, A. Sugamoto, M. Z. Yang, and Y. D. Yang, Phys. Rev. D **62**, 094020 (2000); D. S. Du, D. S. Yang, and G. H. Zhu, Phys. Rev. D **64**, 014036 (2001); Phys. Lett. B **509**, 263 (2001); **488**, 46 (2000); H. Y. Cheng and K. C. Yang, Phys. Lett. B **511**, 40 (2001); Phys. Rev. D **64**, 074004 (2001); **63**, 074011 (2001); D. S. Du, H. J. Gong, J. F. Sun, D. S. Yang, and G. H. Zhu, Phys. Rev. D **65**, 074001 (2002); J. F. Sun, G. H. Zhu, and D. S. Du, Phys. Rev. D **68**, 054003 (2003); X. Q. Li, G. R. Lu, and Y. D. Yang, Phys. Rev. D **68**, 114015 (2003); **71**, 019902 (E) (2005).
- [10] M. Z. Yang and Y. D. Yang, Phys. Rev. D **62**, 114019 (2000).
- [11] D. S. Du, H. J. Gong, J. F. Sun, D. S. Yang, and G. H. Zhu, Phys. Rev. D **65**, 094025 (2002); **66**, 079904 (E) (2002).
- [12] M. Beneke and M. Neubert, Nucl. Phys. B **675**, 333 (2003).
- [13] X. Q. Li and Y. D. Yang, Phys. Rev. D **72**, 074007 (2005).
- [14] D. S. Du, Int. J. Mod. Phys. A **21**, 658 (2006); M. Beneke, Int. J. Mod. Phys. A **21**, 642 (2006).
- [15] W. S. Hou, Nucl. Phys. B **308**, 561(1988); J.-M. Gérard and W. S. Hou, Phys. Rev. Lett. **62**, 855 (1989); Phys. Rev. D **43**, 2909 (1991); Phys. Lett. B **253**, 478 (1991).

- [16] H. Simma and D. Wyler, Nucl. Phys. B **344**, 283 (1990); J. Liu and Y. P. Yao, Phys. Rev. D **41**, 2147 (1990).
- [17] C. Greub and P. Liniger, Phys. Rev. D **63**, 054025 (2001).
- [18] S. W. Bosch and G. Buchalla, Nucl. Phys. B **621**, 459 (2002); M. Beneke, T. Feldmann, and D. Seidel, Nucl. Phys. B **612**, 25 (2001); A. Ali and A. Y. Parkhomenko, Eur. Phys. J. C **23**, 89 (2002); S. Mishima and A. I. Sanda, Prog. Theor. Phys. **110**, 549 (2003).
- [19] G. Eilam and Y. D. Yang, Phys. Rev. D **66**, 074010 (2002).
- [20] N. Cabibbo, Phys. Rev. Lett. **10**, 531 (1963); M. Kobayashi and T. Maskawa, Prog. Theor. Phys. **49**, 652 (1973).
- [21] A. Ali, G. Kramer, and C. D. Lu, Phys. Rev. D **58**, 094009 (1998); **59**, 014005 (1999); Y. H. Chen, H. Y. Cheng, B. Tseng, and K. C. Yang, Phys. Rev. D **60**, 094014 (1999); **62**, 054029 (2000).
- [22] N. G. Deshpande, B. Dutta, and S. Oh, Phys. Lett. B **473**, 141 (2000); M. Gronau, Phys. Rev. D **62**, 014031 (2000); M. Gronau and J. L. Rosner, Phys. Rev. D **61**, 073008 (2000); A. S. Dighe, M. Gronau, and J. L. Rosner, Phys. Rev. D **57**, 1783 (1998).
- [23] G. Buchalla, A. J. Buras, and M. E. Lautenbacher, Rev. Mod. Phys. **68**, 1125 (1996).
- [24] T. Feldmann and T. Hurth, J. High Energy Phys. **11**, 037 (2004).
- [25] H. Y. Cheng, H. n. Li and K. C. Yang, Phys. Rev. D **60**, 094005 (1999).
- [26] Heavy Flavour Averaging Group, <http://www.slac.stanford.edu/xorg/hfag>.
- [27] A. J. Buras, R. Fleischer, S. Recksiegel, and F. Schwab, Phys. Rev. Lett. **92**, 101804 (2004); Nucl. Phys. B **697**, 133 (2004).
- [28] W. M. Sun, Phys. Lett. B **573**, 115 (2003); C. W. Chiang, arXiv: hep-ph/0502183.
- [29] R. Fleischer and T. Mannel, Phys. Rev. D **57**, 2752 (1998); A. J. Buras and R. Fleischer, Eur. Phys. J. C **11**, 93 (1999); **16**, 97 (2000).

- [30] M. Beneke and S. Jager, arXiv: hep-ph/0512351.
- [31] H-n. Li, S. Mishima, and A. I. Sanda, Phys. Rev. **72**, 114005 (2005); H-n. Li and S. Mishima, arXiv: hep-ph/0602214.
- [32] A. R. Williamson and J. Zupan, arXiv:hep-ph/0601214; C. W. Bauer, I. Z. Rothstein and I. W. Stewart, arXiv:hep-ph/0510241; C. W. Bauer, D. Pirjol, I. Z. Rothstein and I. W. Stewart, Phys. Rev. D **70**, 054015 (2004).
- [33] A. J. Buras, P. Gambino, U. A. Haisch, Nucl. Phys. B **570**, 117 (2000).
- [34] S. Eidelman, *et al.*, Phys. Lett. B **592**, 1 (2004).
- [35] CDF Collaboration, arXiv:hep-ex/0507091.
- [36] L. Wolfenstein, Phys. Rev. Lett. **51**, 1945 (1983).
- [37] J. Charles *et al.* [CKMfitter Group], Eur. Phys. J. C **41**, 1 (2005), updated results and plots available at: <http://ckmfitter.in2p3.fr>.
- [38] S. Narison, arXiv:hep-ph/0510108.
- [39] M. Beneke and T. Feldmann, Nucl. Phys. **B592**, 3 (2001).
- [40] P. Ball and V. M. Braun, Phys. Rev. D **58**, 094016 (1998); P. Ball, J. High Energy Phys. **09**, 005 (1998); V. M. Braun and I. E. Filyanov, Z. Phys. C **48**, 239 (1990).
- [41] V. M. Braun, D. Y. Ivanov, and G. P. Korckemsky, Phys. Rev. D **69**, 034014 (2004); A. Khodjamirian, T. Mannel, and N. Offen, Phys. Lett. B **620**, 52 (2005).
- [42] A. Gray *et al.* [HPQCD Collaboration], Phys. Rev. Lett. **95**, 212001 (2005).
- [43] P. Ball and R. Zwicky, Phys. Rev. D **71**, 014015 (2005); **71**, 014029 (2005); Phys. Lett. B **633**, 289 (2006).